

Evolution of Shear-enhanced
Compaction Bands and Pure
Compaction Bands: An example from
the Willunga Basin, South Australia

Thesis submitted in accordance with the requirements of the University of
Adelaide for an Honours Degree in Geology

Samuel Rodney Standish White
October 2014



THE UNIVERSITY
of ADELAIDE

ABSTRACT

Shear-enhanced compaction band (SECB) and pure compaction band (PCB) evolution was constrained at Sellicks Beach, analysing measurements from 247 deformation bands recorded at 12 field locations, from outcrop of the Port Willunga Formation and Heatherdale Shale in the Willunga Basin, South Australia. Three distinct deformation band sets were identified with dominant strike orientations of NW-SE, and subordinate strike orientations of NNW-SSE and WNW-ESE. Sets one and two are defined as two sub-sets of SECBs, forming conjugate sets in outcrops of the Port Willunga Formation. Set three was defined as PCB by definition, forming perpendicular to the maximum principal shortening direction. Deformation bands were further characterised by deformation band style; i) sharp; ii) gradual, and; iii) diffuse, and deformation band fills; i) reorientated bioclasts fill (normal fill); ii) black lithic fill, and; iii) micrite fill.

Deformation band conjugate set dihedral angles, band interactions, microstructural and petrophysical properties were used to define the three generations of deformation bands and their temporal evolution. They were formed in response to rotation of stress orientations during basin formation and reactivation, and inversion of the large-scale Willunga Fault at Sellicks Beach during the Middle Eocene and Pliocene.

Thin sections revealed increasing cataclastic failure in deformation bands analysed, enabling for identification of an evolutionary sequence of; i) diffuse, to; ii) gradual, to; iii) sharp, and finally; iv) black lithic. This sequence demonstrates progressively higher amounts of cataclasis and shear.

Thin sections were further used, as well as core samples to produce porosity values of deformation band types, with reductions of porosity values coinciding with higher amounts of cataclasis and shear. Thus, the Port Willunga Formation at Sellicks Beach provides insight into deformation band characteristics and evolution in carbonate rocks, which have not previously been studied in detail.

KEYWORDS

Shear-enhanced compaction band, Pure compaction band, Willunga Basin, Port Willunga Formation.

TABLE OF CONTENTS

Abstract.....	i
Keywords.....	i
List of Figures.....	3
List of Tables	4
Introduction	5
The Geological Setting of the Willunga Basin.....	8
Lithological descriptions and Geology of Sellicks Beach.....	9
Data and sample collection at sellicks beach, s.a	11
Defromation bands observed at sellicks beach, s.a	14
Deformation Band Sets.....	16
Strike Rotation.....	21
Band Thickness, Frequency and Density	22
Band Thicknesses	22
Frequency and Density	23
Deformation Band Styles and Fills.....	24
Deformation Band Styles	24
Deformation Band Fills	26
Deformation band Petrophysical and microstructural Properties.....	27
Discussion.....	30
Deformation Band Sets.....	30
Deformation Band Set 1	30
Deformation Band Set 2	31
Deformation Band Set 3	32
Controls over Horizontal stress orientations	34
Dispersion and Densities at Sellicks Beach.....	35
Thin Section Petrography and Microstructure of Deformation Bands.....	36
Porosity of Deformation Bands	39
Deformation Band Generation History.....	40
Implications for Reservoir Systems.....	42
Implications for water storage in the Adelaide plain sub-basin	43
Conclusions	44
Acknowledgments	46
References	47

Appendix A: Structural analysis	49
Appendix B: Porosity	55
Appendix C: Extended field mapping	59
Appendix D: Face maps 1 to 5	65
Face map 1	65
Face map 2.....	65
Face map 3.....	66
Face map 4.....	66
Face map 5.....	67

LIST OF FIGURES

Figure 1: Geological map of Sellicks Beach, showing the location of; the Willunga Fault; the Heatherdale Shale; the Port Willunga Formation, and; the Alluvial fan sediments. Figure adapted from Cann et al. (2014)..... 10

Figure 2: Map of Sellicks Beach showing all face maps (FM1 to FM5), grid maps (GM1 to GM3) and field sites studied (FS1 to FS4). Inserts are rose diagrams (with numbers corresponding to face maps, grid maps or field sites on map), which show strike orientations of all planes measured. 15

Figure 3: a) Grid map 1 of a wave-cut platform, correlated to face map 4, showing DB1, DB2 and DB3; DB1 and DB2 are planar and DB3 is anastomosing (wavy) in geometry. b) Close up sketch from face map 1, showing cross-cutting relations between DB1, DB2 and DB3. 18

Figure 4: Stereonets of all DB poles to planes collected at Sellicks Beach (unfolded to bedding) Deformation band sub-sets and set. a) All poles to planes collected at Sellicks Beach (black). b) Sub-set A, all north dipping poles to planes (red). c) Sub-set C, all east dipping poles to planes (black). d) Sub-set B, all south dipping poles to planes (green). e) Sub-set D, all west dipping poles to planes (orange), and deformation band Set 3, near vertical-to-vertical (black). 19

Figure 5: a) Face maps 1–5, digitised and dihedral angle schematic; displaying deformation band set relationships in outcrops of the Port Willunga Formation at Sellicks Beach. a) Deformation Band Set 1 (red), Deformation Band Set 2 (blue) and Deformation Band Set 3 (yellow). b) Mean dihedral angle of Deformation band Set 1. (For an enlarged version of each face map see Appendix C)..... 20

Figure 6: Histogram of deformation band thicknesses for from face map locations 1 to 5 at Sellicks Beach..... 22

Figure 7: Histogram of deformation band frequency from face map locations 1 to 5 at Sellicks Beach. 23

Figure 8: Close up photos of deformation band styles hosted by the Port Willunga Formation at Sellicks Beach. a) Sharp, b) Sharp (Micrite), c) Gradual and d) Diffuse. (Red indicates the inner zone and blue line indicates outer zones) 25

Figure 9: Close up photos of deformation band fills hosted by the Port Willunga Formation at Sellicks Beach. a) Reorientated Bioclasts (Normal fill), b) Black Lithic Fill and c) Micrite Fill. 26

Figure 10: a) Schematic illustration showing the arrangement of the conjugate set in Deformation Band Set 1 to the reactivated and inverted reverse sense Willunga Fault. Sub-set A, dipping north (red). Sub-set B, dipping south (Blue). (Fault, dipping to the north) b) Mean dihedral angle of Deformation band Set 1 and deformation band formation angle to the H_{max} at Sellicks Beach; dihedral angle (red) and deformation band formation angle (blue). 30

Figure 11: Schematic illustration showing the conjugate set arrangement of Deformation Band Set 2 to the Willunga Fault; Sub-set C, dipping east (red), Sub-set D, dipping west (Blue). (Fault, dipping north)..... 32

Figure 12: Schematic block diagram depicting maximum horizontal stress (H_{max}) orientations during the formation of the Willunga Basin and generations of deformation band sets at Sellicks Beach. a) Termination of normal faulting. b) Transpressional phase. c) Onset of inversion. 41

LIST OF TABLES

Table 1: Face map locations with GPS coordinates, length, height and orientation. 12
Table 2: Wave-cut platform grid map locations, correlating face map number, GPS coordinates, length along face map and distance from face map. 12
Table 3: Field site locations with GPS coordinates, south of the Willunga Fault at Sellicks Beach. 12
Table 4: Rock sample locations with GPS coordinates of thin section and core samples. 13
Table 5: Breakdown of Deformation band sets collected from each of the 11 field locations hosted by the Port Willunga Formation at Sellicks Beach..... 14
Table 6:Thin section sample images, descriptions and porosity; and core sample absolute porosity of all rock samples collected at Sellicks Beach. 28

INTRODUCTION

The behaviour of deformation bands and their relationship to faults have become increasingly more significant in the prediction of fluid flow in the subsurface e.g. for hydrocarbon, geothermal, mineral and aquifer systems (Fossen and Bale 2007, Rotevatn et al. 2013). The propensity for deformation bands to act as a baffle to fluid flow or to reorient fluid flow causing compartmentalisation in reservoirs is well recognised (Fossen et al. 2007). The evolution of a deformation band is controlled by several variables including; i) tectonic regime; ii) stress state; iii) confining pressure; iv) porosity; v) permeability; vi) cementation, and; vii) host rock properties (e.g. degree of lithification, mineralogy, grain size, grain shape and sorting).

Deformation bands are millimeter-thick planar zones of strain localization identified in porous granular media, most notably porous sandstones and limestones (Fossen et al. 2007). They are generally concentrated in zones of brittle deformation in the upper crustal tectonic and non-tectonic regimes; observed in damage zones related to faults, gravitational slumps and salt diapirs (Fossen et al. 2007, Rath et al. 2011, Rotevatn et al. 2013, Skurtveit et al. 2014). Deformation bands are commonly associated with reductions of one order of magnitude (with respect to the host rock) and reductions in permeability of zero to six orders of magnitude (Fossen and Bale 2007, Fossen et al. 2007).

When defining deformation bands, two classification schemes are employed; i) kinematics of deformation bands, including compaction, shear, dilation or hybrids of

these types (Aydin et al. 2006, Fossen et al. 2007), and; ii) mechanisms of deformation bands, including disaggregation bands (frictional sliding and grain translocation), cataclastic band (grain crushing, fracturing and interlocking) and diagenetic processes (pressure-solution and cementation bands; Fossen et al. 2007, Skurtveit et al. 2014). Classification by mechanism is dependent on both internal and external conditions (tectonic regime, stress state, confining pressure, porosity, permeability and cementation and host rock properties; Fossen et al. 2007, Skurtveit et al. 2014). Over time several properties are susceptible to physical change through burial depth, lithification and uplift. These altering properties allow for the temporal evolution of deformation bands to be defined (Fossen et al. 2007, Skurtveit et al. 2014).

Conjugate sets are one of the most frequently observable and measured geometric properties of deformation bands sets (Fossen et al. 2007). By measuring a conjugate set's dihedral angle, the angle produced can be used to infer the deformation band types forming and the tectonic regime in which the conjugate set formed (Ballas et al. 2014, Soliva et al. 2013). This technique is commonly linked to deformation band mechanisms, as contributing evidence to the temporal evolution of the deformation bands (Fossen et al. 2007).

Shear-enhanced compaction bands form orientated oblique to the maximum compressional stress (38° to 53°) and are planar over tens of metres in geometry, displaying porosity values within bands of 0.5% to 8.8% hosted by carbonates (Skurtveit et al. 2014, Eichhubl et al. 2010, Cilona et al. 2012). Pure compaction bands form orientated perpendicular to the maximum horizontal stress (H_{\max}) direction in

compressional regimes (90°), are typically wavy in geometry, and commonly display porosity values within bands of 1% and 11% hosted by carbonates (Cilona et al. 2012, Eichhubl et al. 2010, Tondi et al. 2006, Fossen et al. 2011). Both SECBs and PCBs are observed preferentially forming in high differential stress regimes, which are generally associated with compressional thrust-faulting regimes (Soliva et al. 2013, Ballas et al. 2014).

The bulk of previous studies have targeted deformation bands hosted by siliciclastic rocks e.g. (Aydin 1978, Antonellini et al. 1994, Ballas et al. 2014, Fossen et al. 2011, Rotevatn et al. 2013, Sallet and Wibberley 2010), however, only few studies have been conducted on deformation bands hosted by carbonates (Cilona et al. 2012, Rath et al. 2011, Tondi et al. 2006). Therefore, the aim of this study is to use the Port Willunga Formation at Sellicks Beach, a limestone, as a natural laboratory to expand our existing understanding of deformation bands hosted within carbonates.

In this paper, detailed geometric, microstructural and petrophysical properties of deformation bands from the Port Willunga Formation collected from locations at Sellicks Beach are presented. This is achieved by means of detailed field work, collection of structural data and microscopic analysis, as well as porosity analysis of core samples. This will allow the evolutionary aspects of deformation bands in carbonates to be further defined, and will further relate deformation bands to large-scale structures.

THE GEOLOGICAL SETTING OF THE WILLUNGA BASIN

The Willunga Basin is a sub-basin of the St Vincent Basin, located on the south coast of South Australia on the western flank of the Mount Lofty Ranges (Higgs et al. 2012). It is one of several sub-basins formed in the Middle Eocene due to reactivation of north-south trending grabens and half grabens, during final separation between the Australian and Antarctic continents (Holford et al. 2011, Sandiford 2003). The basin structure is a gently seaward-dipping trough, with asymmetric wedge geometry, and Cenozoic sediment successions thickening towards the south. The basin is bounded to the south-east by the Willunga Fault scarp that demonstrates a reverse sense, and the Clarendon Fault Block to the north (Sandiford 2003, Cann et al. 2014).

Three distinct tectonic and depositional phases define the evolution of the Willunga Basin: i) Middle Eocene (~43 Ma) termination of normal faulting, linked to cessation of NW-SE extensional stresses, and a transgressive sequence of non-marine clastic sediments to marine carbonate-dominated successions (Holford et al. 2011, Hillis et al. 2008, Willcox and Stagg 1990); ii) onset of NW-SE compressional stresses and ongoing mild deformation of these Cenozoic sediments during reverse displacement along normal faults that formed during prior extensional event (Holford et al. 2011, Sandiford 2003), and; iii) reactivation and inversion of the Willunga Fault, initiated by E-W orientated H_{\max} orientation at 6 to 8 Ma, facilitating a transition of depositional sequences from mainly carbonate to siliciclastics (Sandiford 2003, Holford et al. 2011, Willcox and Stagg 1990).

Lithological descriptions and Geology of Sellicks Beach

A succession of the Willunga Basin crops out at Sellicks Beach, adjacent the Willunga Fault. It is composed of three non-conformable stratigraphic units; i) Heatherdale Shale; ii) Port Willunga Formation, and; iii) Alluvial fan sediments.

The Heatherdale Shale is Early Cambrian in age, consists of interbedded (dark purple-black) shale and siltstone units, cropping out immediately south of the Willunga Fault in the southern part of the study area. Inversion of the Willunga Fault has exposed ~50 m of the Heatherdale Shale within the up-thrusted hanging wall of the Fault. In response to inversion of Willunga Fault, the Heatherdale Shale exhibits high angle near vertical bedding orientations (~80°).

The Port Willunga Formation is Middle Eocene in age, a bioclastic grainstone consisting of fragmented echinoid, bivalve and bryozoan, cropping out at beach level as low cliff sections and wave-cut platforms. In the northern part of the study area, the unit is nearly horizontal, hosting a gentle anticline, where isolated, clusters and conjugate sets of deformation bands are visible in both low cliff sections and wave-cut platforms. In the southern part of the study area, the Port Willunga Formation is juxtaposed and upturned, possessing high angle bedding orientations (~65 °), unconformably overlying the Heatherdale Shale.

The Alluvial fan sediments Late Pliocene to Early Pleistocene in age, consist of sediments and conglomerates eroded from the Neoproterozoic and Cambrian rocks of Sellicks Hill to the south (Cann et al. 2014). Alluvial fan sediments unconformably overlay the Port Willunga Formation in the northern part of the study area, and both the Heatherdale Shale and Port Willunga Formation in the southern part of the study area.

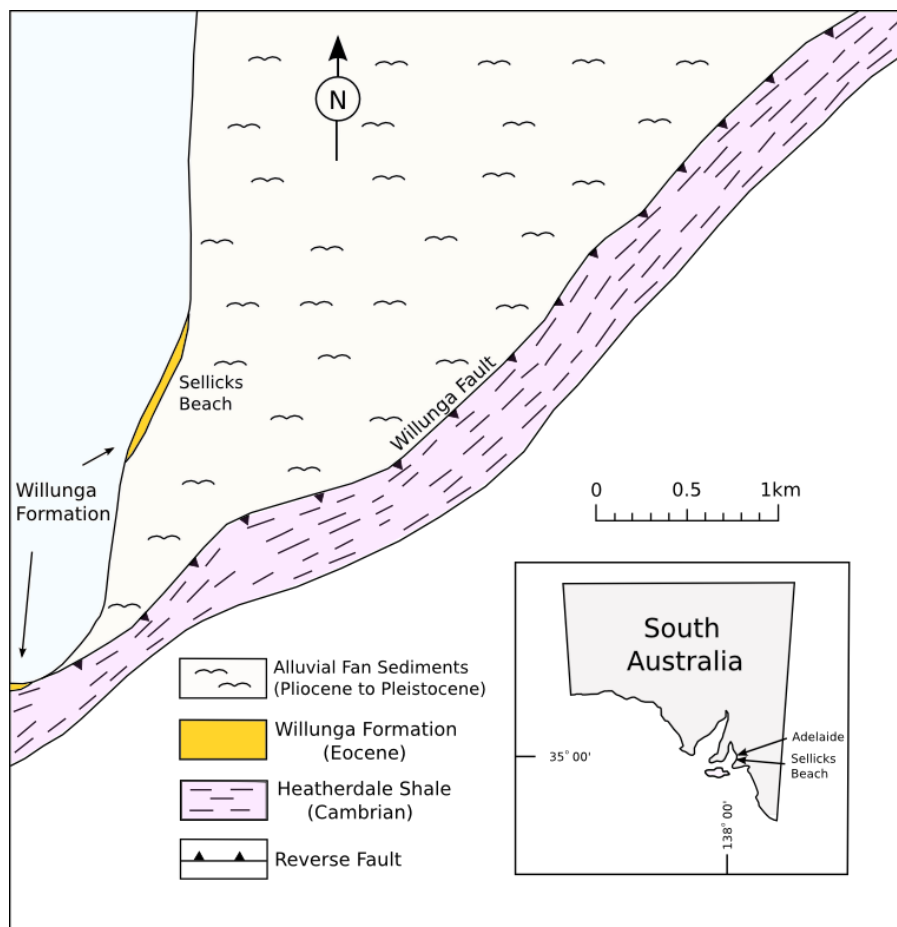


Figure 1: Geological map of Sellicks Beach, showing the location of; the Willunga Fault; the Heatherdale Shale; the Port Willunga Formation, and; the Alluvial fan sediments. Figure adapted from Cann et al. (2014).

DATA AND SAMPLE COLLECTION AT SELLICKS BEACH, S.A

From 12 field locations, including five face maps (Table 1), three grid maps (Table 2) and four field sites (Table 3), field data and samples for structural and microscopic analyses were collected. Face maps (detailed cross-sections, with a scale of 1:1000) covering 80 m² to 210 m² of the vertical cliff sections were constructed and record the characteristics of deformation bands including; i) frequency; ii) location (height and length); iii) dip and dip direction; iv) deformation band width; v) deformation band style, and; vi) fill. All bedding (dip and dip direction) and sedimentary structures were recorded in the face maps. Grid maps (detailed grids, with a scale of 1:1000) covering 25 m² of the wave-cut platforms, measured the strike of deformation bands at Sellicks Beach, at locations where the Port Willunga Formation cropped out (Figure 1). Stereonet 8 (Allmendinger et al. 2013) and JRS Suite© (provided by Ikon Science) was used to construct stereonet and rose diagrams of structural data collected at these sites (see Appendix A for full details).

Eight rock samples collected at various locations (Table 4); where the Port Willunga Formation cropped out as low cliff sections at Sellicks Beach were used to produce eight thin sections and eight core samples. Digital photos from thin sections were used for the image analysis technique using JMicroVision© V1.27 (Roudit 2014) to determine porosity of both the host rock and deformation bands from thin sections. In addition, core samples were used to calculate absolute porosity using a modified Archimedes method (see Appendix B for full details).

Table 1: Face map locations with GPS coordinates, length, height and orientation.

Face map no.	GPS Start		GPS End		Length of Face map	Height of Face map	Orientation of Face map
	Latitude	Longitude	Latitude	Longitude			
Face map 1	-35 ° 20 ' 6.58440 "	138 ° 26 ' 48.21727 "	-35 ° 20 ' 7.48906 "	138 ° 26 ' 48.03039 "	32 m	2.5 m	East 109°
Face map 2	-35 ° 20 ' 10.75013 "	138 ° 26 ' 47.25453 "	-35 ° 20 ' 11.84936 "	138 ° 26 ' 47.06153 "	35 m	3 m	East 092°
Face map 3	-35 ° 20 ' 16.44734 "	138 ° 26 ' 45.05550 "	-35 ° 20 ' 19.21507 "	138 ° 26 ' 42.43381 "	33.5 m	6 m	East 113°
Face map 4	-35 ° 20 ' 20.36995 "	138 ° 26 ' 41.80340 "	-35 ° 20 ' 21.16643 "	138 ° 26 ' 41.10507 "	33 m	4 m	East 124°
Face Map 5	-35 ° 20 ' 24.11721 "	138 ° 26 ' 39.46761 "	-35 ° 20 ' 25.24468 "	-35 ° 20 ' 25.24468 "	35 m	3 m	East 124°

Table 2: Wave-cut platform grid map locations, correlating face map number, GPS coordinates, length along face map and distance from face map.

Grid map no.	Correlating Face map no.	GPS Location		Length along Face map	Distance from Face map
		Latitude	Longitude		
Grid map 1	4	-35 ° 20 ' 20.62330 "	138 ° 26 ' 39.97372 "	28 m – 33 m	31 m
Grid map 2	4	-35 ° 20 ' 20.23834 "	138 ° 26 ' 40.18386 "	15 m – 20 m	32 m
Grid map 3	5	-35 ° 20 ' 25.05490 "	138 ° 26 ' 37.77474 "	30 m – 35 m	31 m

Table 3: Field site locations with GPS coordinates, south of the Willunga Fault at Sellicks Beach.

Field Site no.	GPS Locations	
	Latitude	Longitude
Field Site 1	-35 ° 21 ' 11.57562 "	138 ° 25 ' 58.91710 "
Field Site 2	-35 ° 21 ' 10.11362 "	138 ° 26 ' 4.94434 "
Field Site 3	-35 ° 21 ' 10.30133 "	138 ° 26 ' 7.67142 "
Field Site 4	-35 ° 21 ' 10.62882 "	138 ° 26 ' 10.86939 "

Table 4: Rock sample locations with GPS coordinates of thin section and core samples.

Rock Sample no.	Thin Section Sample	Core Sample	GPS Locations	
			Longitude	Latitude
1	7H	Core 2A	-35 ° 20 ' 22.28888 "	138 ° 26 ' 40.47567 "
2	8H	N/A	-35 ° 20 ' 10.16558 "	138 ° 26 ' 47.23333 "
3	1G	Core 1G	-35 ° 20 ' 24.44066 "	138 ° 26 ' 39.41781 "
4	2G	N/A	-35 ° 20 ' 10.16558 "	138 ° 26 ' 47.23333 "
5	5S	Core 1S and 2S	-35 ° 20 ' 10.16726 "	138 ° 26 ' 47.31248 "
6	6S	Core 3S and 4S	-35 ° 20 ' 6.67918 "	138 ° 26 ' 48.09548 "
7	3B	Core 1B	-35 ° 20 ' 12.79063 "	138 ° 26 ' 47.07150 "
8	4B	N/A	-35 ° 20 ' 6.72081 "	138 ° 26 ' 48.52978 "

DEFROMATION BANDS OBSERVED AT SELLICKS BEACH, S.A

Two hundred and forty-seven deformation bands were identified and recorded from twelve field locations; five face maps, three wave-cut platforms and four field sites in the Willunga Basin where the Port Willunga Formation and Heatherdale Shale Formation cropped out (Figure 2). From these measurements three deformation bands sets and four sub-sets were identified; a breakdown of the deformation band sets is shown in Table 5.

Table 5: Breakdown of Deformation band sets collected from each of the 11 field locations hosted by the Port Willunga Formation at Sellicks Beach.

Set no.	Sub-set	Deformation Band count	Observed in (*FM and *FS)	Strike	Dip Direction	Dip	Fill (*N, *M and *BL)
Deformation Band Set 1	A	73	FM 1-5 and FS 1	NWW-ESE	North	Moderate to Steep	N, M, BL
	B	42	Pervasive	WNW-ESE	South	Variable	N, M, BL
Deformation Band Set 2	C	57	FM 1-5 and FS 1-2	NNW-SSE	East	Variable	N, M, BL
	D	22	FM 1-5, FS 1 and 3	NNW-SSE	West	Moderate to Steep	N and BL
Deformation Band Set 3	N/A	42	FM 1-5 and FS 3	NW-SE	N/A	Steep (80 to 90°)	N and M

***FM = Face Map and *FS = Field Site, *N = Normal, *M = Micrite, *BL = Black Lithic.**

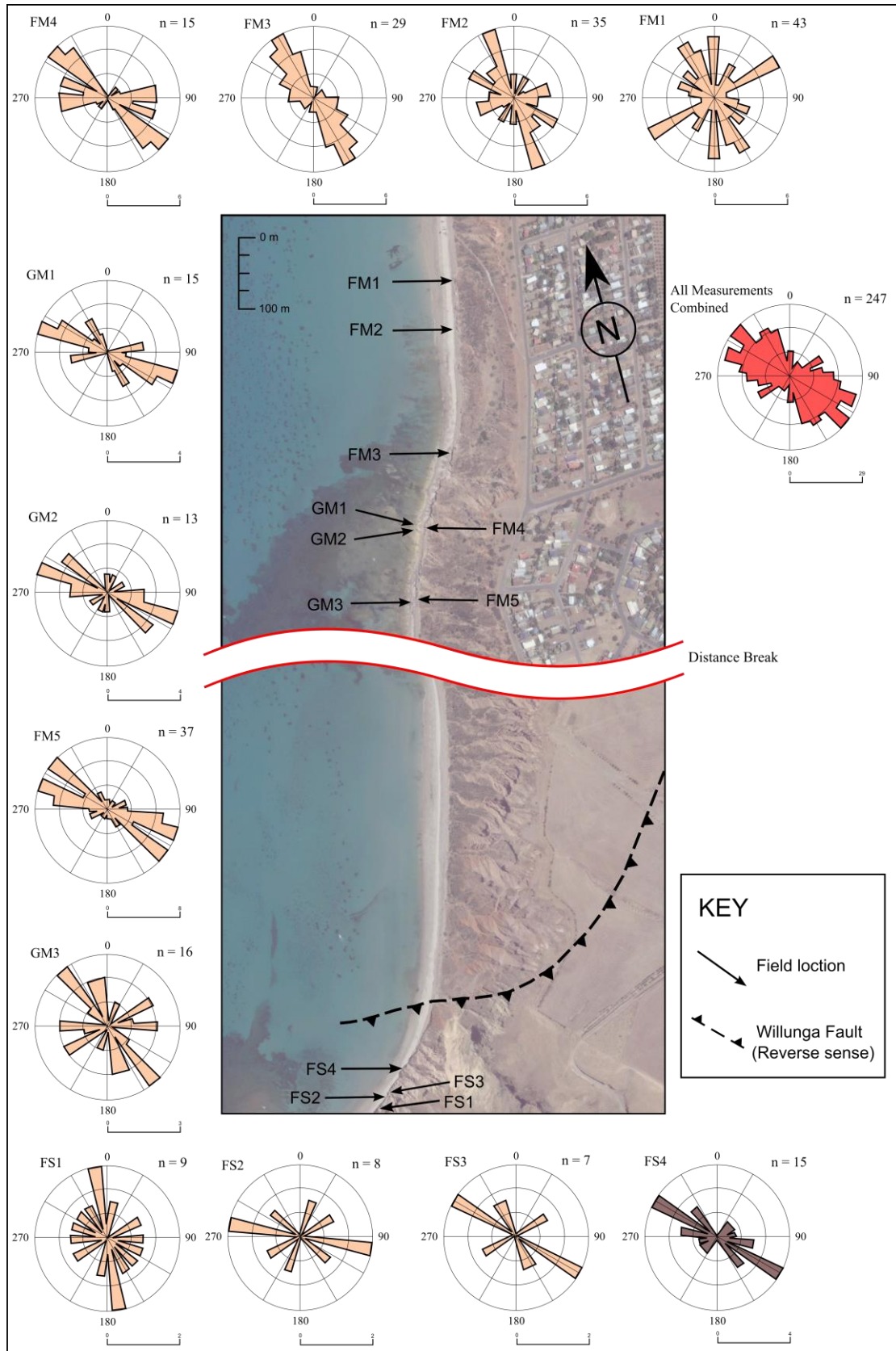


Figure 2: Map of Sellicks Beach showing all face maps (FM1 to FM5), grid maps (GM1 to GM3) and field sites studied (FS1 to FS4). Inserts are rose diagrams (with numbers corresponding to face maps, grid maps or field sites on map), which show strike orientations of all planes measured.

Deformation Band Sets

Deformation Band Set 1 (DB1) consists of sub-sets A and B (table 5), together sub-set A and B define a conjugate set. The conjugate set is observed with one sub-set dipping north (sub-set A) and one dipping south (sub-set B; Figure 4). The dihedral angle of the conjugate set was observed progressively tightening from face maps 1 to 5 (north to south), and had a mean dihedral angle was 59° (Figure 5 a, b). In outcrops of cliff sections the number of deformation bands became progressively more frequent to the south (towards face map 5; Figure 5, a) and commonly formed clusters of bands, separated by periods of low deformation band numbers. Within outcrops of wave-cut platforms the set was planar over meters (Figure 3, a).

Deformation Band Set 2 (DB2) is made up of sub-sets C and D (Table 5), together sub-set C and D define a conjugate set. The conjugate set is observed with one sub-set dipping east (sub-set C) and one dipping west (sub-set D; Figure 4). In outcrops of cliff sections the number of deformation bands became progressively more frequent to the north (towards face map 1) and commonly formed clusters of bands, separated by periods of low deformation band numbers (Figure 5, a). The set was planar over meters in wave-cut platforms that correlated to face maps produced (Figure 3, a).

Deformation and Set 3 (DB3) was observed having near vertical-to-vertical dip (80° to 90°). In outcrops of cliff section deformation bands are observed vertical in clusters of deformation band conjugates sets and as individual deformation bands in areas of low band numbers (Figure 5, a). In outcrops of wave-cut platforms deformation bands were observed anastomosing, being wavy in nature (Figure 3, a). In outcrops of cliff sections

the number of deformation bands became progressively more frequent to the south (towards face map 5), although, the highest frequency of deformation bands was recorded in face map three (Figure 5, a).

Cross cutting relationships were observed between the three sets of deformation bands in face map 1, and a close up sketch produced (Figure 3, b). The sketch, displays offsets between DB1 and DB2, whereby DB1 has cross-cut DB2 (Figure 3, a). The sketch also shows DB3 being cross-cut by CS1 (Figure 3, b).

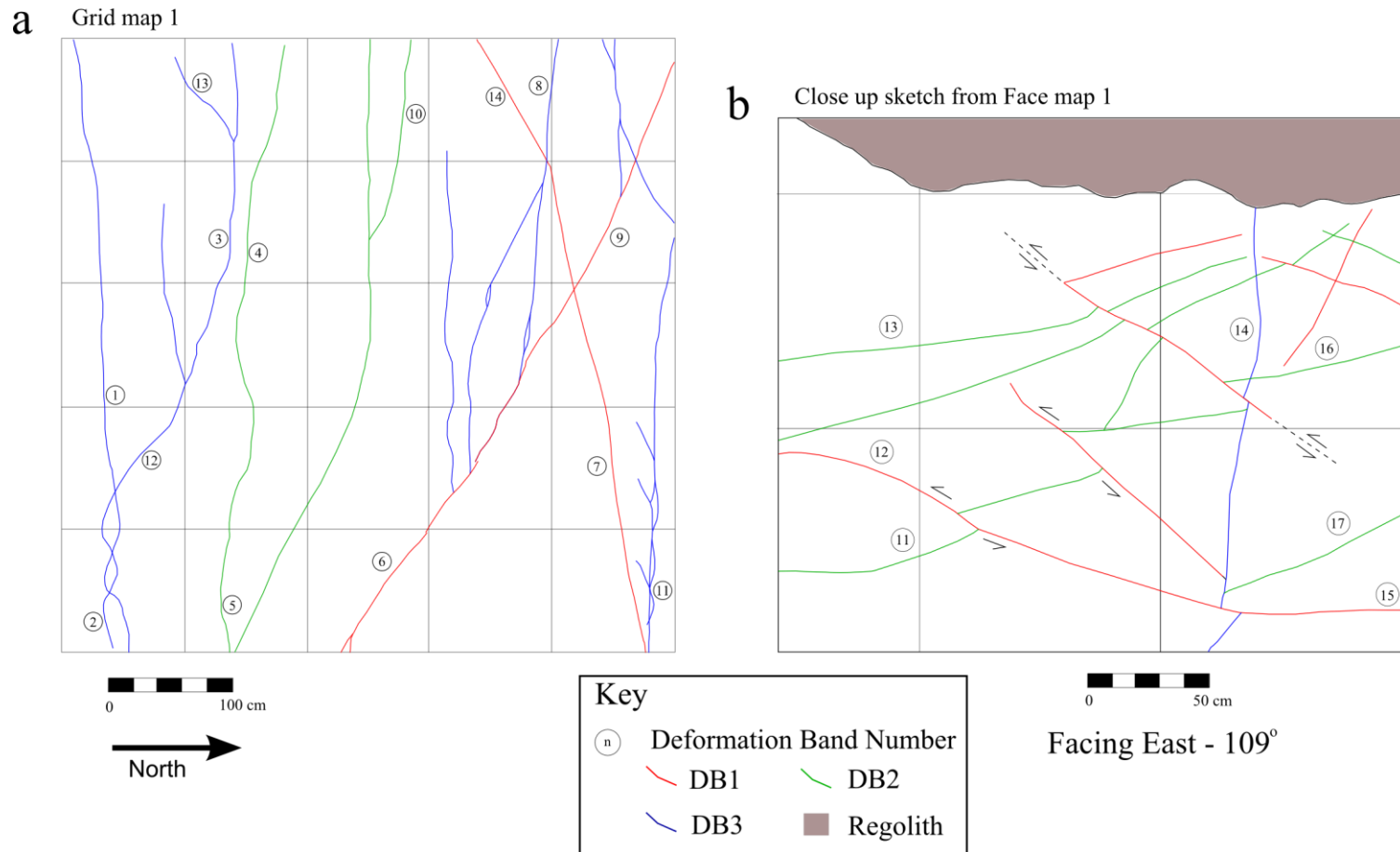


Figure 3: a) Grid map 1 of a wave-cut platform, correlated to face map 4, showing DB1, DB2 and DB3; DB1 and DB2 are planar and DB3 is anastomosing (wavy) in geometry. b) Close up sketch from face map 1, showing cross-cutting relations between DB1, DB2 and DB3.

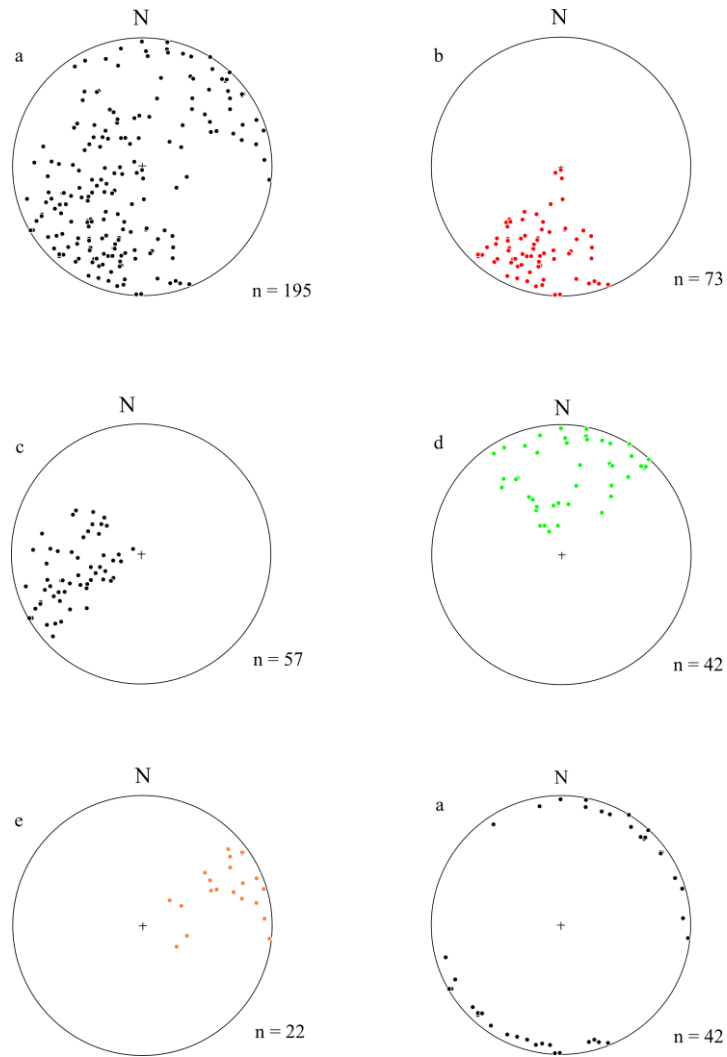


Figure 4: Stereonets of all DB poles to planes collected at Sellicks Beach (unfolded to bedding) Deformation band sub-sets and set. a) All poles to planes collected at Sellicks Beach (black). b) Sub-set A, all north dipping poles to planes (red). c) Sub-set C, all east dipping poles to planes (black). d) Sub-set B, all south dipping poles to planes (green). e) Sub-set D, all west dipping poles to planes (orange), and deformation band Set 3, near vertical-to-vertical (black).

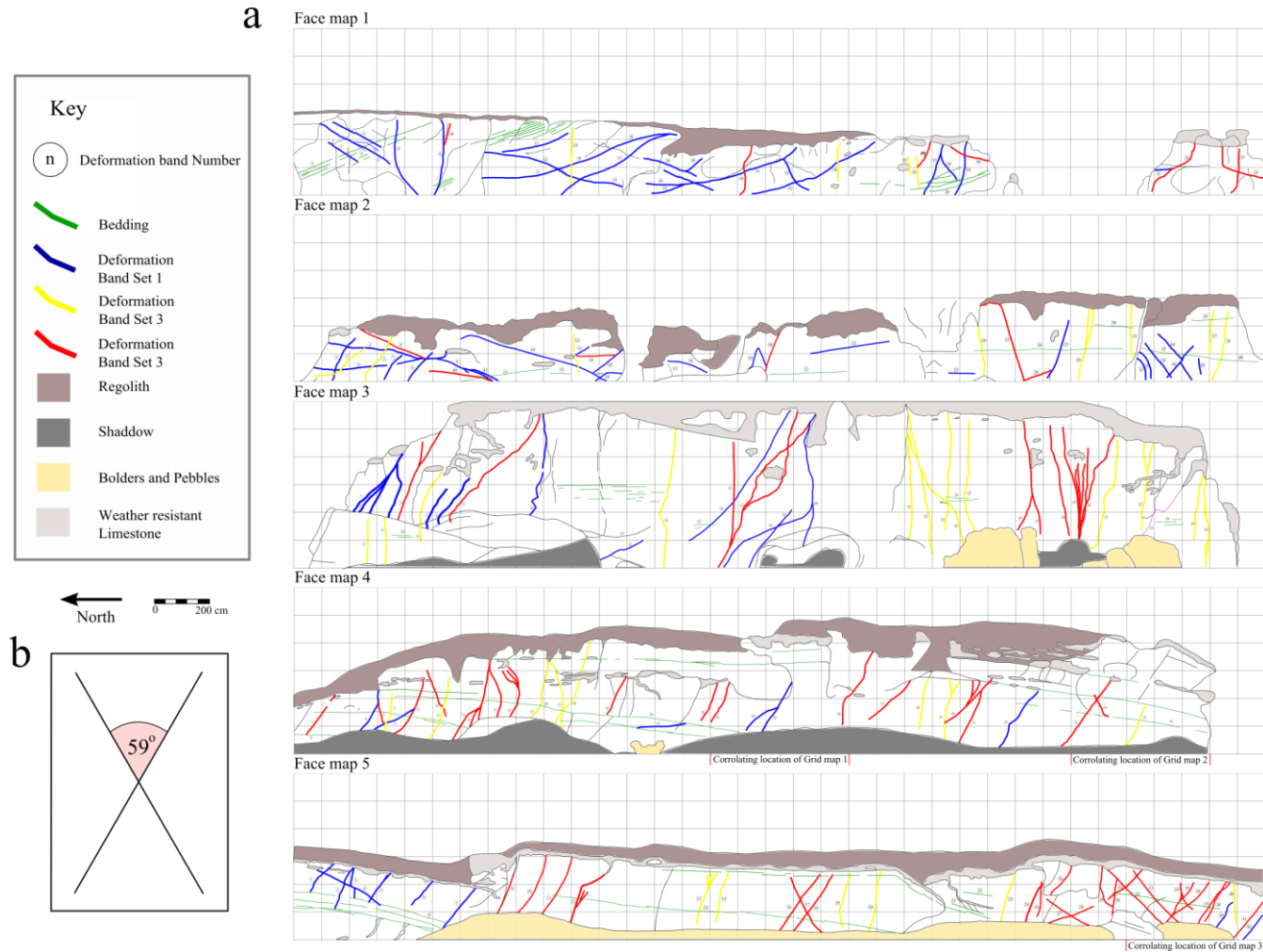


Figure 5: a) Face maps 1–5, digitised and dihedral angle schematic; displaying deformation band set relationships in outcrops of the Port Willunga Formation at Sellicks Beach. a) Deformation Band Set 1 (red), Deformation Band Set 2 (blue) and Deformation Band Set 3 (yellow). b) Mean dihedral angle of Deformation band Set 1. (For an enlarged version of each face map see Appendix C).

Strike Rotation

From all field locations, strike measurements were collected and plotted in a series of rose diagrams (Figure 2). In face maps 1 to 5, rose diagrams (FM1, FM2, FM3, FM4 and FM5) display a gradual rotation of deformation band strike orientations from NNW-SSE to WNW-ESE (Figure 2). Strike orientations were observed rotating from NNW-SSE in FM1 (most northerly), to WNW-ESE strike orientations in FM5 (most southerly) as face maps progressed closer to the Willunga Fault (Figure 2).

Grid maps produced corresponding to face maps 4 and 5, plotted as rose diagrams (GM1, GM2 and GM3) were observed displaying NW-SE strike orientations, correlating with face map strike orientations, rose diagrams FM4 and FM5 (Figure 2).

In field sites 1 - 4, located in the hanging wall of the Willunga Fault, rose diagrams (FS1, FS2, FS3 and FS4) were collected from cliff sections where the Port Willunga Formation and Heatherdale Shale cropped out. Strike orientations were observed rotating from NNW-SSE in FS1 (most southerly), to WNW-ESE strike orientations in FS4 (most northerly), as the field sites progressed closer to the Willunga Fault (Figure 2).

A rose diagram of all 12 combined field locations displays a dominant strike orientation of NW-SE, and subordinate strike orientations of NNW-SSE and WNW-ESE (All measurements combined; Figure 2).

Band Thickness, Frequency and Density

BAND THICKNESSES

The thickness of each deformation band from face maps 1 to 5 was measured and collected (Figure 6). The band thicknesses display right skewed normal distribution, with the maximum at 1 – 2 mm.

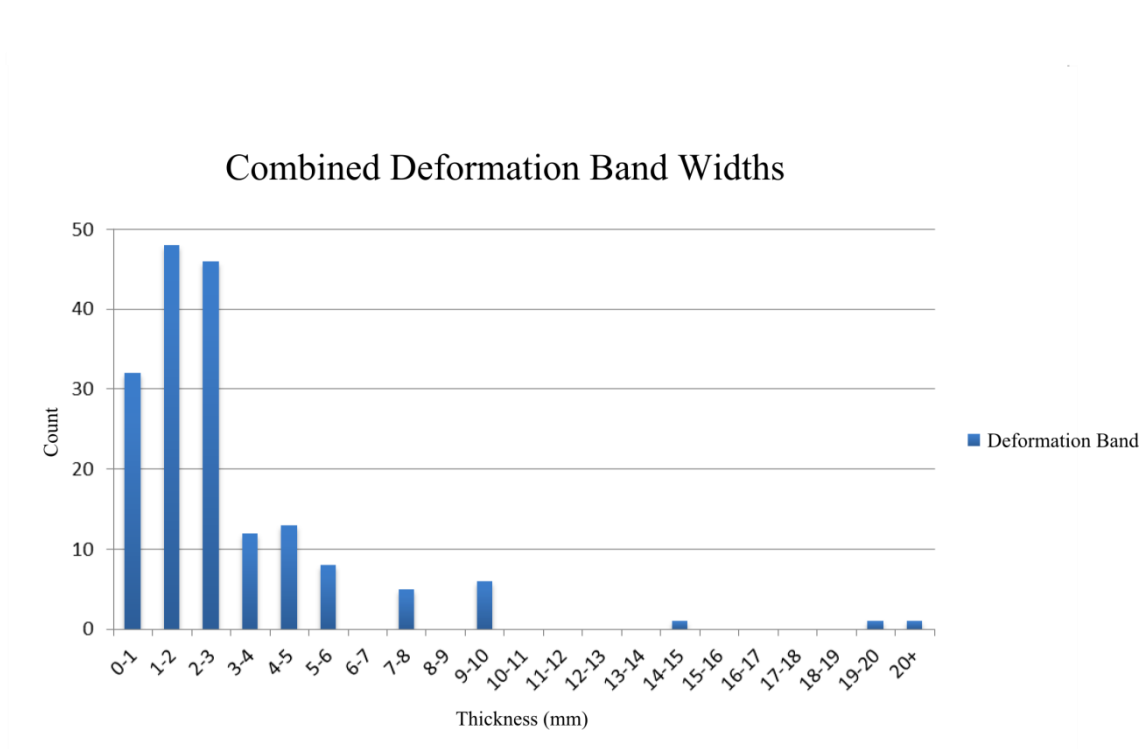


Figure 6: Histogram of deformation band thicknesses for from face map locations 1 to 5 at Sellicks Beach.

FREQUENCY AND DENSITY

For face maps 1 to 5 deformation band frequency was graphed, presented in Figure (7), and densities were measured. The mean band sum for face maps 1 to 5 was 40.1, with the greatest quantity of bands observed in face map 1 (48 bands). Mean band density for face maps 1 to 5 is 1.2 bands/m, with the greatest density measured in Face map one (1.4 bands/m).

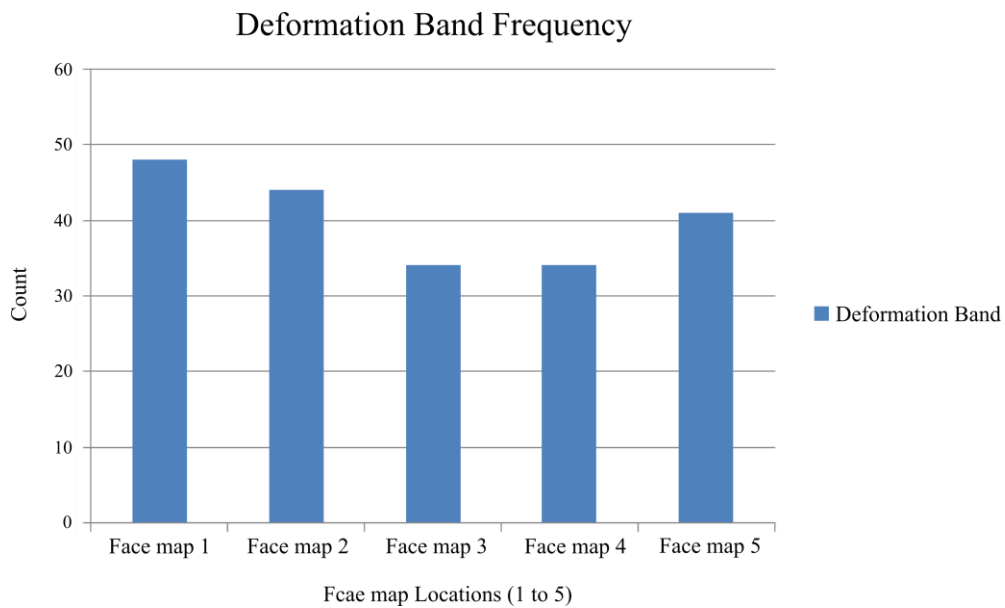


Figure 7: Histogram of deformation band frequency from face map locations 1 to 5 at Sellicks Beach.

Deformation Band Styles and Fills

DEFORMATION BAND STYLES

Three deformation band styles were observed at Sellicks Beach hosted by the Port Willunga Formation; i) sharp; ii) gradual, and; iii) diffuse (Figure 8). Sharp deformation band style, defined by; i) a distinct visual change from randomly orientated bioclasts too aligned bioclasts within the deformation band aperture zone (Figure 8, a), and; ii) a distinct change in lithology between deformation band and host rock e.g. a deformation band containing micrite infill and a bioclastic grainstone host rock (Figure 8, b).

Gradual deformation band style, defined by obvious zones within the deformation band's width, an inner zone containing distinct alignment of bioclasts and outer zones where bioclasts display sub-alignment, although, still distinct from host rock (Figure 8, c).

Diffuse deformation band style was defined by aligned to sub-aligned bioclasts within the inner zone of the deformation band, and poorly distinguishable outer zones of irregularly aligned bioclasts, which grade into the host rock (Figure 8, d).

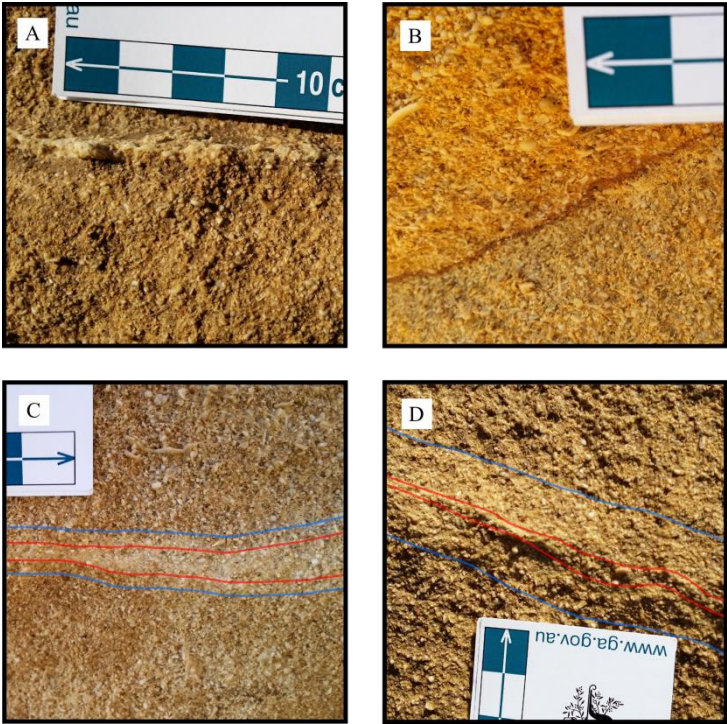


Figure 8: Close up photos of deformation band styles hosted by the Port Willunga Formation at Sellicks Beach. a) Sharp, b) Sharp (Micrite), c) Gradual and d) Diffuse. (Red indicates the inner zone and blue line indicates outer zones)

DEFORMATION BAND FILLS

Three deformation band fills were observed at Sellicks Beach hosted by the Port Willunga Formation (Figure 9). They are classified as; i) reorientated bioclasts (normal fill); ii) black lithic fill, and; iii) micrite fill. Normal fill, defined by weathered bioclasts reorientated in alignment with respect to one another under hand lens (Figure 9, a). Black lithic fill, defined by inclusions of black lithics within reorientated bioclast deformation bands, predominantly observed within weathered zones along bands (Figure 9, b). Micrite fill, defined by silt to clay sized particles occasionally containing small amounts of bioclasts, predominantly observed hosted by sharp style deformation bands (Figure 9, c).

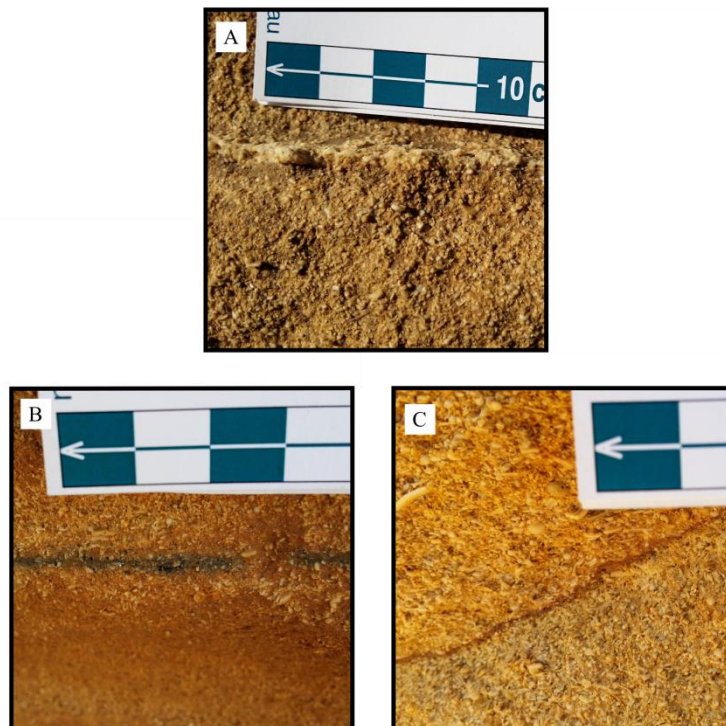


Figure 9: Close up photos of deformation band fills hosted by the Port Willunga Formation at Sellicks Beach. a) Reorientated Bioclasts (Normal fill), b) Black Lithic Fill and c) Micrite Fill.

DEFORMATION BAND PETROPHYSICAL AND MICROSTRUCTURAL PROPERTIES

From eight rock samples collected at Sellicks Beach, eight thin sections and eight core samples were produced (Table 6). Thin sections provide detailed petrography and microstructural analysis of host rock and deformation bands, identifying the main deformation band mechanisms operating. Core samples were used to calculate absolute porosity, using a modified Archimedes method (Table 6).

Table 6: Thin section sample images, descriptions and porosity; and core sample absolute porosity of all rock samples collected at Sellicks Beach.

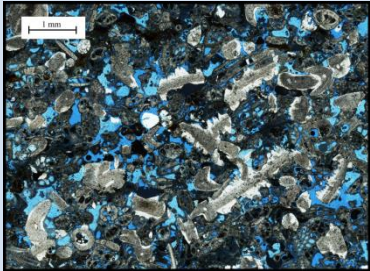
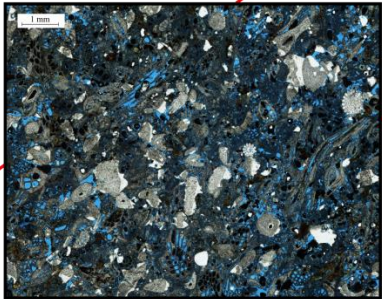
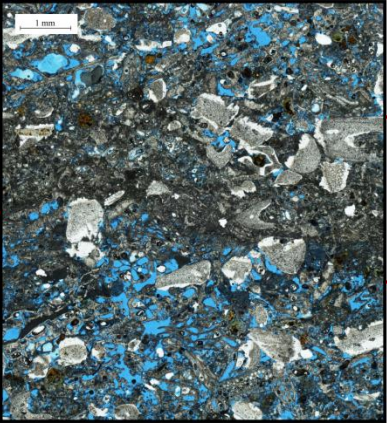
Thin section sample	Thin section Description	Thin Section Porosity	Core sample (Absolute) Porosity
Sample 7H and 8H (Host Rock) 	<p>Highly porous bioclastic carbonate grainstone; moderately to poorly sorted, consisting of rounded to sub-rounded broken clasts of echinoderms and fragmented bivalves, less than 0.5 mm in size. As well as angular to very angular clasts of fragmented bivalves, bryozoans and corals (fibros lattice like in structure), ranging from 0.5 to 1 mm in size (some up to 2 mm).</p> <ul style="list-style-type: none"> - Bivalves are light speckled grey in colour, commonly rimmed by a white border and have high relief than smaller fragmented clasts. - The samples are observed having no cemented clasts. 	<p>Primary porosity is observed between clasts and bryozoans, where chambers or soft parts have remained unfilled during burial.</p> <p>Porosity generated using JMicroVision was 15.77 % for sample 7H and 20.29 % for sample 8H.</p>	<p>Core 2A (Host Rock):</p> <p>Absolute porosity: 35.1 %</p>
Sample 1G and 2G (Gradual Deformation band) 	<p>Gradual deformation band, characterised by a deformation band width of 3.5 to 4.5 mm. Displaying minor compaction and interlocking between bryozoan and coral clasts, as well as lack of cemented clasts.</p> <ul style="list-style-type: none"> - Visually, little reduction in pore space sizes within the bands zone compared to surrounding host rock. - Minor alignment of elongate clasts (corals and bivalves), rotated with their long axis paralleling the band orientation. - Red lines indicate deformation band thickness. 	<p>Porosity generated for 1G was 5.17 %.</p> <p>Porosity generated for 2G was 6.15 %.</p>	<p>Core 1G (Gradual Deformation Band):</p> <p>Absolute porosity: 31.2%</p>

Table 6: continued

Thin section sample	Thin section Description	Thin Section Porosity	Core sample (Absolute) Porosity
<p>Sample 5S and 6S (Sharp Deformation band)</p> 	<p>Sharp deformation band, characterised by a deformation band widths of predominantly 2 mm, high compaction and interlocking of bryozoan and coral clasts, accompanied by crushing and lack of cementation of clast.</p> <ul style="list-style-type: none"> - Large bivalves and foraminifer clasts (grey in colour) 0.5 to 1 mm in sizes have higher relief than small broken clast. - Alignment of elongate bivalve clasts, rotated with their long axis paralleling the band orientation observed on the borders of the band (e.g. top and bottom right margins of the band). - Red lines indicate deformation band thickness. - Visually reduction in pores within the band, compared to the surrounding host rock. - 	<p>Porosity generated for 5S was 4.56 %.</p> <p>Porosity generated for 6S was 2.79 %.</p>	<p>Core 1S, 2S, 3S and 3S (Sharp Deformation Bands):</p> <p>Absolute porosity: 32.55 %</p> <p>Absolute porosity: 33.2 %</p> <p>Absolute porosity: 35.9 %</p> <p>Absolute porosity: 35.5 %</p>
<p>Sample 3B and 4B (Black Lithic)</p> 	<p>Black Lithic deformation band was characterised by a deformation band widths of 2.5 mm, displaying moderate to high compaction, crushing, small amounts clast cracking and lack of cemented clasts.</p> <ul style="list-style-type: none"> - Highly reduced broken angular clasts of 100 to 50 µm in size, was observed suspended in a black matrix throughout the band. - Large clasts (bivalves grey in colour) 0.5 to 1 mm in sizes displayed higher relief than small broken clasts. - Alignment of elongate clasts (small and large) rotated with their long axis paralleling band orientation, observed in the centre and band margins. - Visually reduction in pores within the band, compared to the surrounding host rock. - Red lines indicate deformation band thickness. - *Blue channel visible to the left of the image is a result of thin section staining. 	<p>Porosity generated for 3B was 1.75 %.</p> <p>Porosity generated for 4B was 1.75 %.</p>	<p>Core 1B (Black Lithic Deformation Band):</p> <p>Absolute porosity: 32.5 %</p>

DISCUSSION

Deformation Band Sets

DEFORMATION BAND SET 1

Deformation band set 1 consisting of sub-sets A and B striking NWN-ESE, and forms a conjugate set. The set is interpreted to have formed during N-S compressional stresses associated with the reverse sensed Willunga Fault. However, the mean dihedral angle of the conjugate set displays traditional normal faulting ranges, between 40° and 60° , associated with extension, coinciding with observations by Ballas et al. (2014).

Traditional extensional dihedral angles at Sellicks beach are interpreted to have formed in response to the preservation of high angle dip after reactivation and inversion of the Willunga Fault (Figure 10, a).

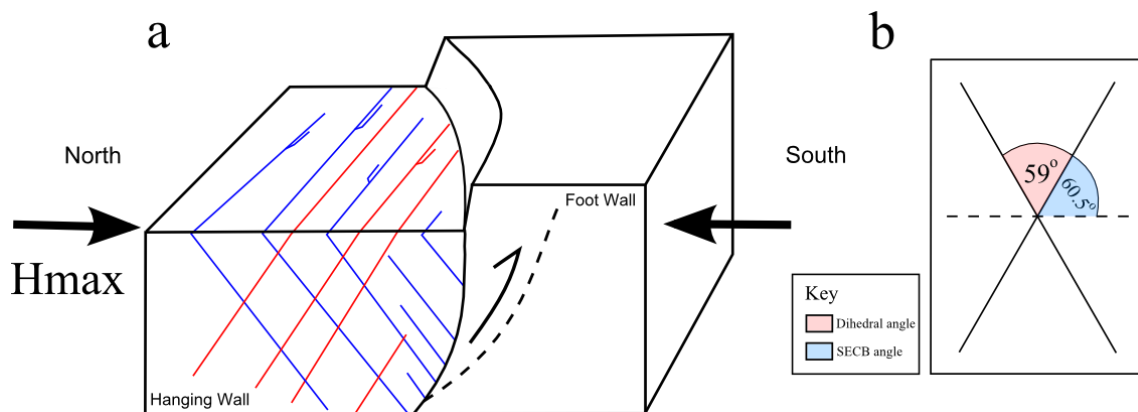


Figure 10: a) Schematic illustration showing the arrangement of the conjugate set in Deformation Band Set 1 to the reactivated and inverted reverse sense Willunga Fault. Sub-set A, dipping north (red). Sub-set B, dipping south (Blue). (Fault, dipping to the north) b) Mean dihedral angle of Deformation band Set 1 and deformation band formation angle to the H_{max} at Sellicks Beach; dihedral angle (red) and deformation band formation angle (blue).

Additional to this, evidence for SECB evolution was exhibited in DB1 coinciding with Eichhubl et al. (2010) and Ballas et al. (2014), who observe SECBs predominantly forming at an oblique angle, between 32° and 58° to the H_{\max} in compressional regimes. The formation of SECBs at Sellicks Beach is interpreted to have formed after a rotation of the H_{\max} of about 60° from NW-SE to N-S. The mean dihedral angle of DB1 is 59° , thus the set is orientated about 60.5° to N-S H_{\max} at Sellicks Beach (Figure 10, b). Additionally to this, added supporting evidence for SECB evolution is observed in outcrops of wave-cut platforms, where deformation bands of DB1 are planar over meters (Figure 3, a); coinciding with observations by Fossen et al. (2007), who observed SECB planar over tens of meters in outcrop.

DEFORMATION BAND SET 2

Deformation band set 2 consisting of sub-set C and D striking N-S, and forms a conjugate set. The set possess dip directions perpendicular to the strike of the Willunga Fault; sub-set C, dipping east, and sub-set D, dipping west (Figure 11). The deformation band set is discordant with traditional normal faulting conjugate set geometries, where two sets of deformation bands dip in opposite directions at an oblique angle and strike sub-parallel to an associated fault (Fossen and Bale 2007). The orientations of DB2 are interpreted to be produced during a transpressional phase, during which the set formed at an oblique angle to the Willunga Fault (Figure 11).

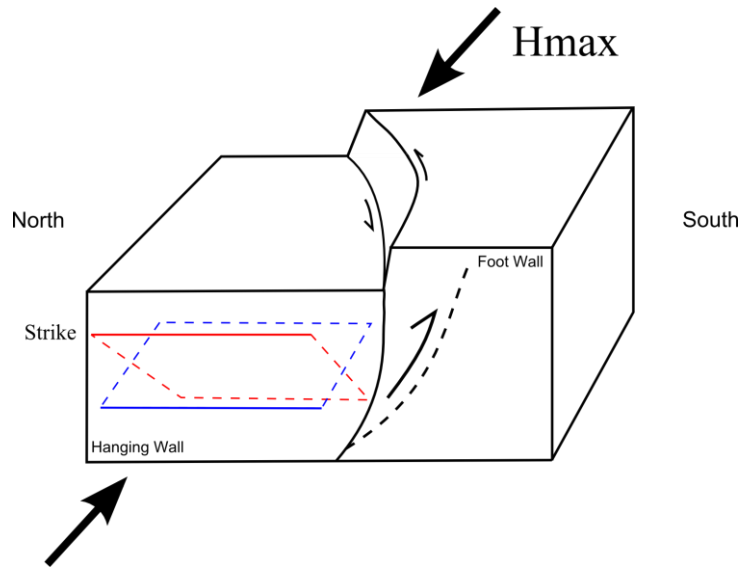


Figure 11: Schematic illustration showing the conjugate set arrangement of Deformation Band Set 2 to the Willunga Fault; Sub-set C, dipping east (red), Sub-set D, dipping west (Blue). (Fault, dipping north)

Additional to this, DB2 exhibited evidence of SECB evolution, observed in outcrops of wave-cut platforms being planar over meters (Figure 3, a); coinciding with observations by (Fossen et al. 2007).

DEFORMATION BAND SET 3

Deformation Band Set 3 strikes NW-SE, interpreted to be PCB by definition, forming after a rotation of the H_{max} at Sellicks Beach by about 45° from NW-SE to N-S orientation. Studies by Tondi et al. (2006) and Eichhubl et al. (2010) observed PCBs forming perpendicular to the H_{max} in compressional regimes and wavy in geometry in outcrop. Deformation band set 3 coincides with these studies, observed in outcrops of cliff sections vertically intersecting conjugate sets of DB1 and DB2 (Figure 5). This symmetry between sets allows for the interpretation that DB3 formed perpendicular to the H_{max} at Sellicks Beach. Additional to this, DB3 in outcrops of wave-cut platforms are anastomosing (wavy) in nature (Figure 3, a).

Deformation band cross-cutting relationships observed between all the deformation band sets are interpreted to represent a generational hierarchy forming at Sellicks Beach, following an evolutionary sequence of; i) DB2; ii) DB3, and; iii) DB1 (Figure 3, b).

Different deformation band set orientation further suggest possible generations of deformation bands forming at Sellicks Beach in response to the deformation history experienced by the Willunga Basin. Possibly allowing deformation band types forming to be linked to stress orientations experienced at Sellicks Beach.

Controls over Horizontal stress orientations

Strike orientations at Sellicks Beach progressively rotate from NNW-SSE to NWN-ESE in face map 1-5 (north to south) and in field sites 1-4 (south to north; Figure 2). Rotation and alignment of deformation band set strike orientations provide a possible connection between deformation band generations and deformation bands types formed at Sellicks Beach. Strike orientations of deformation bands form perpendicular to the H_{\max} (Fossen et al. 2007).

First-order stress controls are generated at plate boundaries and transferred into continent interiors (Hillis et al. 2008, Zoback 1992). Second-order stress controls are regional in effect, often associated with lithostatic flexure (Zoback 1992). Third-order stress controls are local in effect, often produced by slumps and faults (Zoback 1992, Bell 1996). Rotation of deformation band sets strike orientations to a uniform NW-SE strike at Sellicks Beach is interpreted to be consequence of third-order local structural controls produced by the Willunga Fault. This interpretation is in line with observations by Zoback (1992) and Yale et al. (1994), who observe structural controls produced by faults extending up to two kilometers in distance.

Dispersion and Densities at Sellicks Beach

Face maps and grid maps produced from the Willunga Formation provide an opportune example to compare large-scale fault deformation band dispersion and densities to previous studies.

Previous studies state that; i) deformation band distributions in compressional regimes are generally well dispersed, whereas deformation bands in extensional regimes tend to be localised more proximal to an associated fault, and; ii) higher deformation band densities are observed more proximal to a fault reflecting higher strain values closer to the fault (Skurtveit et al. 2014, Fossen and Hesthammer 1997, Ballas et al. 2014).

Deformation bands at Sellicks are observed coinciding with the first statement, possessing high dispersion, forming at a distance about two kilometres from the Willunga fault (Figure 2). However, deformation bands at Sellicks Beach contradict the second statement, observed having the highest band densities observed in face map 1 (most distal to the Willunga Fault; Figure 5). Higher deformation band densities in face map one are interpreted to be a result of the intermediate transpressional phase, during which DB2 was formed. Further evidence for this interpretation is observed by majority of DB2 being located in face maps one and two, distal from the Willunga Fault (Figure 5).

Thin Section Petrography and Microstructure of Deformation Bands

Thin sections of eight rock samples collected from the Port Willunga Formation at Sellicks Beach provide an opportunity to compare petrographic and microstructural observations from thin sections to previous studies e.g. (Aydin 1978, Rath et al. 2011, Fossen et al. 2007, Aydin et al. 2006, Solum et al. 2010). This will allow possible links to be made to larger-scale deformation band mechanisms controlling deformation band types forming at Sellicks Beach.

Deformation bands formed at Sellicks Beach are interpreted to be cataclastic by definition. Cataclastic deformation bands described by Aydin (1978) and Fossen et al. (2007) occur when mechanical grain failure is a significant deformation mechanism (grain fracturing, crushing and interlocking), commonly observed evolving from disaggregation to cataclastic failure. Increase in cataclastic failure is commonly a function of; i) strain hardening, caused by cementation of host rock; ii) increased differential stress, and; iii) high confining pressure (Aydin et al. 2006, Fossen et al. 2007). As cataclastic failure increases, higher amounts of grain crushing and fracturing of grains is experienced, coinciding with a wide grain size distribution, increased matrix and decreases of deformation band thickness (Solum et al. 2010, Aydin et al. 2006).

Within carbonates, specifically limestone, precipitation of cement is frequently observed (Choquette and James 1987). As a result of precipitation of cement in bioclastic limestones deformation bands can possess higher yield strengths, altering the dominant deformation mechanism from disaggregation to cataclasis (Rath et al. 2011).

Host rock thin sections 8H and 7H act as a control to which thin sections of deformation band styles and deformation band fills may be compared (Table 6). Host samples are characterised by; i) lack of cementation of clasts; ii) a combination of rounded to sub-rounded fragmented clasts and angular to very angular clasts ranging from 0.5 to 2 mm; and, iii) high porosity values of 20.29 % (8H) and 15.77 % (7H) respectively (Table 6).

Gradual deformation band style, thin sections 1G and 2G; exhibiting deformation band widths between 3.5 to 4.5 mm, minor compaction of clasts, lack of cementation and a reductions in porosity between 10% and 15% (Table 6).

Sharp deformation band style, thin sections 5S and 6S display more classical cataclastic features; characterised by band widths of 2 mm, high compaction and interlocking between clasts, lack of cementation and reductions in porosity between 11% and 17% (Table 6).

Black Lithic deformation band fill, thin sections 3B and 4B exhibit moderate cataclastic band properties. Exhibiting crushing, small amounts of clast cracking (fracturing), wide grain size distribution (1000 to 50 μm) set in black matrix, lack of cementation and reductions in porosity between 14% and 18% (Table 6).

From these observations, deformation bands at Sellicks Beach are interpreted to follow an evolutionary sequence of; i) diffuse; ii) gradual; iii) sharp, and; iv) black lithic, progressively moving from low to moderate cataclasis. Furthermore, deformation band

thickness is interpreted to act as a function of increased cataclasis. Whereby, deformation band thicknesses' decrease coinciding with increased cataclastic failure.

Low to moderated cataclastic failure of deformation bands at Sellicks Beach is interpreted to be consequence of shallow burial (low confining pressure) and lack of cementation of the Port Willunga Formation. Additionally, higher amounts of cataclasis exhibited in deformation bands containing zones of Black Lithic fill is interpreted to be caused from precipitation of heavy minerals most likely iron oxide and/or hydroxides, coinciding with (Rotevatn et al. 2008). The precipitation of heavy minerals is interpreted to have increase intragranular yield strength of grains, causing strain hardening, localizing higher amounts of cataclasis in deformation bands, agreeing with Rath et al. (2011) and Aydin et al. (2006).

Additional to this, deformation bands analysed in thin section display minor amounts of shear motion following the same evolutionary sequence aforementioned. Evidence of shear motion is exhibited by the rotation and alignment of clasts, becoming progressively more established from thin sections 1G and 2G, which displays minor rotation and alignment; too, thin sections 3B and 4B, which exhibit moderate to high alignment of elongate clasts, in the centre and band margins (Table 6); coinciding with Fossen et al. (2007), Rotevatn et al. (2008) and Soliva et al. (2013).

POROSITY OF DEFORMATION BANDS

Thin section sample porosity and core sample absolute porosities collected from Sellicks Beach were compared with studies of deformation bands hosted by limestone by Rath et al. (2011) and Cilona et al. (2012). These studies documented microscopic porosity reductions in cataclastic deformation bands between 12% and 21%, with respect to the host rock, and core sample absolute porosity reductions between 15% and 20%.

Reductions in thin section samples from the Willunga Formation coincided with these values, displaying porosity reductions between 10% and 18% with respect to the host rock (Table 6). The porosity reductions in thin sections were observed following the same evolutionary sequence aforementioned, becoming increasingly less porous coinciding with increased cataclastic deformation.

Absolute porosity values of deformation band core samples collected at Sellicks Beach disagree with these observations, showing negligible reductions in absolute porosity (Table 6). However, samples measured show consistency, with all samples (including the host sample) displaying absolute porosities between 31.2% and 35.9%. Low reductions and consistency of measurements causing negligible results are interpreted to be the result of large core volume, with respect to deformation band sample size.

Additionally, large differences between thin section and core sample porosity values is interpreted to be attributed to thin sections only representing two dimensional properties

of pore space, compared to core samples which are representative of the three dimensional characteristics of pore space.

Deformation Band Generation History

The timing of deformation band generations at Sellicks Beach is constrained based on deformation events and deformation band set orientations within the St Vincent and Willunga Basin.

- 1) Middle Eocene (~43 Ma) NW-SE compressional stress reactivated the north-south trending normal faulting graben complex of the St Vincent Basin, creating accommodation space for the deposition of the Port Willunga Formation (Sandiford 2003, Holford et al. 2011; Figure 12). Deposition of the Port Willunga Formation into the accommodation space commenced in the Middle Miocene (Holford et al. 2011).

- 2) Continued NW-SE compressional stress, instigating ongoing mild deformation of Cenozoic sediments, during reverse displacement along normal faults that formed during prior to extension (Dewhurst et al. 2002, Higgs et al. 2012). Continued NW-SE compressional stresses in the Willunga Basin are interpreted to have caused an intermediated transpressional phase at Sellicks Beach, during which DB2 formed at an oblique angle to the Willunga Fault (Figure 12).

- 3) Increased compressional stress prior to 6 to 8 Ma inversion is interpreted to have resulted in third-order local structural control over horizontal maximum stresses associated with the Willunga Fault. Whereby, the H_{\max} at Sellicks Beach rotated

by about 45° from NW-SE to N-S orientation, after which DB3 is interpreted to have formed (Figure 12). During onset of inversion of the Willunga Fault at a 6 to 8 Ma increases in differential stresses are interpreted to result in the formation of DB1.

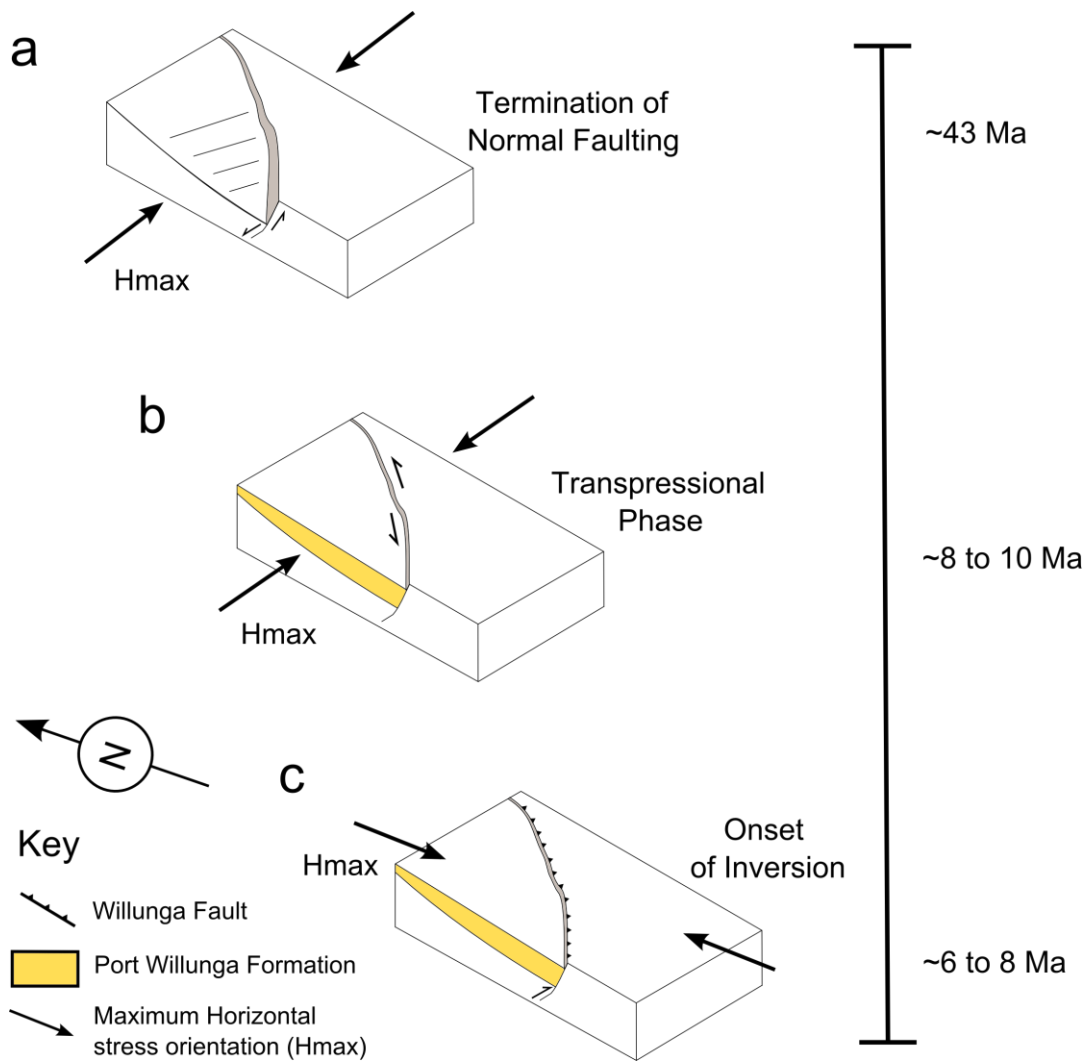


Figure 12: Schematic block diagram depicting maximum horizontal stress (H_{max}) orientations during the formation of the Willunga Basin and generations of deformation band sets at Sellicks Beach. a) Termination of normal faulting. b) Transpressional phase. c) Onset of inversion.

Implications for Reservoir Systems

Deformation bands commonly result in reduced permeability of porous rocks, however, the impact this has on fluid flow remains unclear in literature (Fossen and Bale 2007, Rotevatn et al. 2013). Although, it has been previously suggested that deformation bands in siliciclastic reservoirs may act as a seal, the capacity of low porosity deformation band clusters to act as a seal is now redundant (Fossen et al. 2007, Fossen and Bale 2007). Deformation bands have the potential to act as a baffle to fluid flow and to reorient fluid flow, potentially causing compartmentalization within reservoir systems (Fossen and Bale 2007).

Deformation bands hosted by carbonates are observed reducing porosity and permeability by larger magnitudes to that of deformation bands hosted by siliciclastic sediments, possibly a control of cementation (Rath et al. 2011). After cementation of host rock and deformation bands, grains or clasts possess higher intragranular yield strength, commonly resulting in strain hardening causing increased cataclasis (Aydin et al. 2006, Fossen et al. 2007). Implying that higher reductions observed in carbonates could be linked to their ability to readily undergo cementation at low burial depths, which is not possible for siliciclastic sediments.

Therefore the potential for deformation bands to act as baffle or reorient fluid flow in carbonate reservoirs is more likely, potentially causing greater amounts of compartmentalization. By increasing literature on deformation bands hosted by carbonates the potential for them to act as positive indicators for migration pathways is plausible.

IMPLICATIONS FOR WATER STORAGE IN THE ADELAIDE PLAIN SUB-BASIN

The Port Willunga Formation Aquifer of the Adelaide Plain Sub-Basin is generally high yielding (Pavelic et al. 2008). Currently the aquifer is being utilized for irrigation at McLaren Vale and its greater surrounding areas (Stewart 2007). Observation wells within the basin identified a stressed area, where decline in water levels is recognised. The stressed area has been named Fractured Rock Reservoir, observed outcropping adjacent the Willunga Fault at Onkaparinga Gorge. Water level and flow patterns in this area are observed being highly variable, strongly influenced by the size and densities of fractures in outcrops.

It is interpreted that ‘fractures’ at this location are in reality deformation bands, formed associated with the adjacent Willunga fault. Whereby, high deformation band densities in outcrop are acting to baffle and reorient fluid flow, causing in compartmentalization in the aquifer. This interpretation highlights the need for further analogs of deformation bands hosted by carbonates.

CONCLUSIONS

The purpose of this study was to use the Port Willunga Formation at Sellicks Beach as a natural laboratory to expand our existing understanding of deformation bands hosted within carbonates. After detailed geometric, microstructural and petrophysical analysis of deformation bands, it is evident that three generations of deformation bands sets formed at Sellicks Beach, consequence of third-order local structural control, associated with the Willunga Fault;

- Deformation Band Set 1, consisting of sub-sets A and B striking NNW-ESE, forming a conjugate set, interpreted to be SECB by definition.
- Deformation Band Set 2, consisting of sub-set C and D striking N-S, and forming a conjugate set, interpreted to be SECB by definition.
- Deformation Band Set 3, striking NW-SE, interpreted to be PCB by definition.

This study has shown that three generations of deformation band sets formed during three stages of deformation linked to the Willunga Fault; i) transpression, forming DB2; ii) rotation of H_{\max} by about 45° from NNW-SSE to N-S, forming DB3, and; iii) 6 to 8 Ma onset of inversion of the Willunga Fault, forming DB1.

Rotation and alignment of deformation band set strike orientations is interpreted to be consequence of third-order local structural control, associated with the Willunga Fault.

Microscopic observations identified an evolutionally sequence between deformation bands of; i) diffuse; ii) gradual; iii) sharp, and; iv) black lithic, whereby, decreases in porosity coincided with increased cataclastic deformation and shear motion.

The potential for deformation bands in carbonate reservoirs to act as a baffle to fluid flow and to reorient fluid flow is higher than that of deformation bands in siliciclastic reservoirs, highlighting the need for further analogs of deformation bands hosted by carbonates.

ACKNOWLEDGMENTS

I would first and foremost like to thank my supervisor Dr Rosalind King and secondary supervisor, Dr Simon Holford for their ongoing support throughout the year. Nick Eckert, Gilby Jepson and Andrew White for their assistance in the field work. Dr Themis Carageorgos for assistance and use of laboratory facilities at ASP. I would also like to thank my fellow colleagues Jesse Clark, Rachel Rudd and Bryony Crowe for ongoing technical support. Thanks to S³ for constructive feedback during the year. Thanks to Ikon Science for their use of JRS Suite© and Pontifex & Associates Pty. Ltd. for making thin sections.

REFERENCES

- ALLMENDINGER R. W., CARDOZO N. & FISHER D. 2013. Stereonet 8 v. 8.0.0.
- ANTONELLINI M. A., AYDIN A. & POLLARD D. D. 1994. Microstructure of deformation bands in porous sandstones at Arches National Park, Utah. *Journal of Structural Geology* 16, 941-959.
- AYDIN A. 1978. Small faults formed as deformation bands in sandstone. *pure and applied geophysics* 116, 913-930.
- AYDIN A., BORJA R. I. & EICHHUBL P. 2006. Geological and mathematical framework for failure modes in granular rock. *Journal of Structural Geology* 28, 83-98.
- BALLAS G., SOLIVA R., BENEDICTO A. & SIZUN J. P. 2014. Control of tectonic setting and large-scale faults on the basin-scale distribution of deformation bands in porous sandstone (Provence, France). *Marine and Petroleum Geology*.
- BELL J. 1996. Petro geoscience 2. In situ stresses in sedimentary rocks (part 2): applications of stress measurements. *Geoscience Canada* 23.
- CANN J., LOWER C. & JAGO J. 2014. Provenance and sediment characteristics of contemporary gravel deposits at Sellicks Beach, eastern shore of Gulf St Vincent, South Australia. *Australian Journal of Earth Sciences*, 1-18.
- CHOQUETTE P. W. & JAMES N. P. 1987. Diagenesis# 12. Diagenesis in Limestones-3. The deep burial environment. *Geoscience Canada* 14.
- CILONA A., BAUD P., TONDI E., AGOSTA F., VINCIGUERRA S., RUSTICHELLI A. & SPIERS C. J. 2012. Deformation bands in porous carbonate grainstones: Field and laboratory observations. *Journal of Structural Geology* 45, 137-157.
- DEWHURST D. N., JONES R. M., HILLIS R. R. & MILDREN S. D. 2002. Microstructural and geomechanical characterisation of fault rocks from the Carnarvon and Otway basins. *APPEA journal*.
- EICHHUBL P., HOOKER J. N. & LAUBACH S. E. 2010. Pure and shear-enhanced compaction bands in Aztec Sandstone. *Journal of Structural Geology* 32, 1873-1886.
- FOSSEN H. & BALE A. 2007. Deformation bands and their influence on fluid flow. *AAPG bulletin* 91, 1685-1700.
- FOSSEN H. & HESTHAMMER J. 1997. Geometric analysis and scaling relations of deformation bands in porous sandstone. *Journal of Structural Geology* 19, 1479-1493.
- FOSSEN H., SCHULTZ R. A., SHIPTON Z. K. & MAIR K. 2007. Deformation bands in sandstone: a review. *Journal of the Geological Society* 164, 755-769.
- FOSSEN H., SCHULTZ R. A. & TORABI A. 2011. Conditions and implications for compaction band formation in the Navajo Sandstone, Utah. *Journal of Structural Geology* 33, 1477-1490.
- HIGGS K. E., KING P. R., RAINE J. I., SYKES R., BROWNE G. H., CROUCH E. M. & BAUR J. R. 2012. Sequence stratigraphy and controls on reservoir sandstone distribution in an Eocene marginal marine-coastal plain fairway, Taranaki Basin, New Zealand. *Marine and Petroleum Geology* 32, 110-137.
- HILLIS R. R., SANDIFORD M., REYNOLDS S. D. & QUIGLEY M. C. 2008. Present-day stresses, seismicity and Neogene-to-Recent tectonics of Australia's 'passive' margins: intraplate deformation controlled by plate boundary forces. *Geological Society, London, Special Publications* 306, 71-90.
- HOLFORD S., HILLIS R. R., DUDDY I. R., GREEN P. F., STOKER M., TUITT A., BACKÉ G., TASSONE D. R. & MACDONALD J. 2011. Cenozoic post-breakup compressional deformation and exhumation of the southern Australian margin. *APPEA Journal* 51, 613-638.
- PAVELIC P., DILLON P., BARRY K., ARMSTRONG D., HODSON A., CALLAGHAN J. & GERGES N. 2008. Lessons Drawn from Attempts to Unclog an ASR Well in an Unconsolidated Sand Aquifer.
- RATH A., EXNER U., TSCHEGG C., GASEMANN B., LANER R. & DRAGANITS E. 2011. Diagenetic control of deformation mechanisms in deformation bands in a carbonate grainstone. *AAPG bulletin* 95, 1369-1381.
- RODUI N. 2014 *JMicroVision*, Geneva.
- ROTEVATN A., SANDVE T., KEILEGAVLEN E., KOLYUKHIN D. & FOSSEN H. 2013. Deformation bands and their impact on fluid flow in sandstone reservoirs: the role of natural thickness variations. *Geofluids* 13, 359-371.
- ROTEVATN A., TORABI A., FOSSEN H. & BRAATHEN A. 2008. Slipped deformation bands: a new type of cataclastic deformation bands in Western Sinai, Suez rift, Egypt. *Journal of Structural Geology* 30, 1317-1331.

- SAILLET E. & WIBBERLEY C. A. J. 2010. Evolution of cataclastic faulting in high-porosity sandstone, Bassin du Sud-Est, Provence, France. *Journal of Structural Geology* 32, 1590-1608.
- SANDIFORD M. 2003. Neotectonics of southeastern Australia: linking the Quaternary faulting record with seismicity and in situ stress. *Geological Society of America Special Papers* 372, 107-119.
- SKURTVEIT E., BALLAS G., FOSSEN H., TORABI A., SOLIVA R. & PEYRET M. 2014. Sand textural control on shear-enhanced compaction band development in poorly-lithified sandstone.
- SOLIVA R., SCHULTZ R. A., BALLAS G., TABOADA A., WIBBERLEY C., SAILLET E. & BENEDICTO A. 2013. A model of strain localization in porous sandstone as a function of tectonic setting, burial and material properties; new insight from Provence (southern France). *Journal of Structural Geology* 49, 50-63.
- SOLUM J. G., BRANDENBURG J., NARUK S. J., KOSTENKO O. V., WILKINS S. J. & SCHULTZ R. A. 2010. Characterization of deformation bands associated with normal and reverse stress states in the Navajo Sandstone, Utah. *AAPG bulletin* 94, 1453-1475.
- STEWART S. 2007 McLaren Vale prescribed wells area groundwater monitoring status report 2005. Department of Water, Land and Biodiversity Conservation, Australia, South.
- TONDI E., ANTONELLINI M., AYDIN A., MARCHEGIANI L. & CELLO G. 2006. The role of deformation bands, stylolites and sheared stylolites in fault development in carbonate grainstones of Majella Mountain, Italy. *Journal of Structural Geology* 28, 376-391.
- WILLCOX J. B. & STAGG H. M. J. 1990. Australia's southern margin: a product of oblique extension. *Tectonophysics* 173, 269-281.
- YALE D. P., RODRIGUEZ J., MERCER T. B. & BLAISDELL D. W. 1994. In-situ stress orientation and the effects of local structure-Scott Field North Sea. *Rock Mechanics in Petroleum Engineering*.
- ZOBACK M. L. 1992. First and second order patterns of stress in the lithosphere: The world stress map project. *Journal of Geophysical Research: Solid Earth (1978–2012)* 97, 11703-11728.

APPENDIX A: STRUCTUREAL ANALYSIS

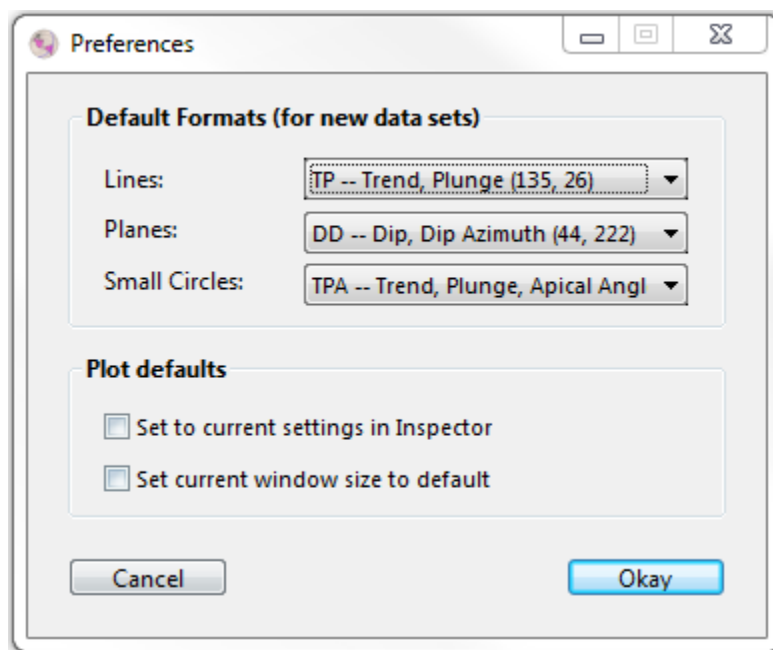
Structural analysis:

In this study, data obtained from the field areas were viewed as stereonet in order to determine possible deformation band sets within the field area. Stereonets were created using Stereonet 8© (Allmendinger et al. 2013) to plot dip and dip directions of bedding and deformation band planes and poles to bedding and poles to deformation band planes in order to interpret fracture networks in the Port Willunga Formation.

Stereonet 8© method -

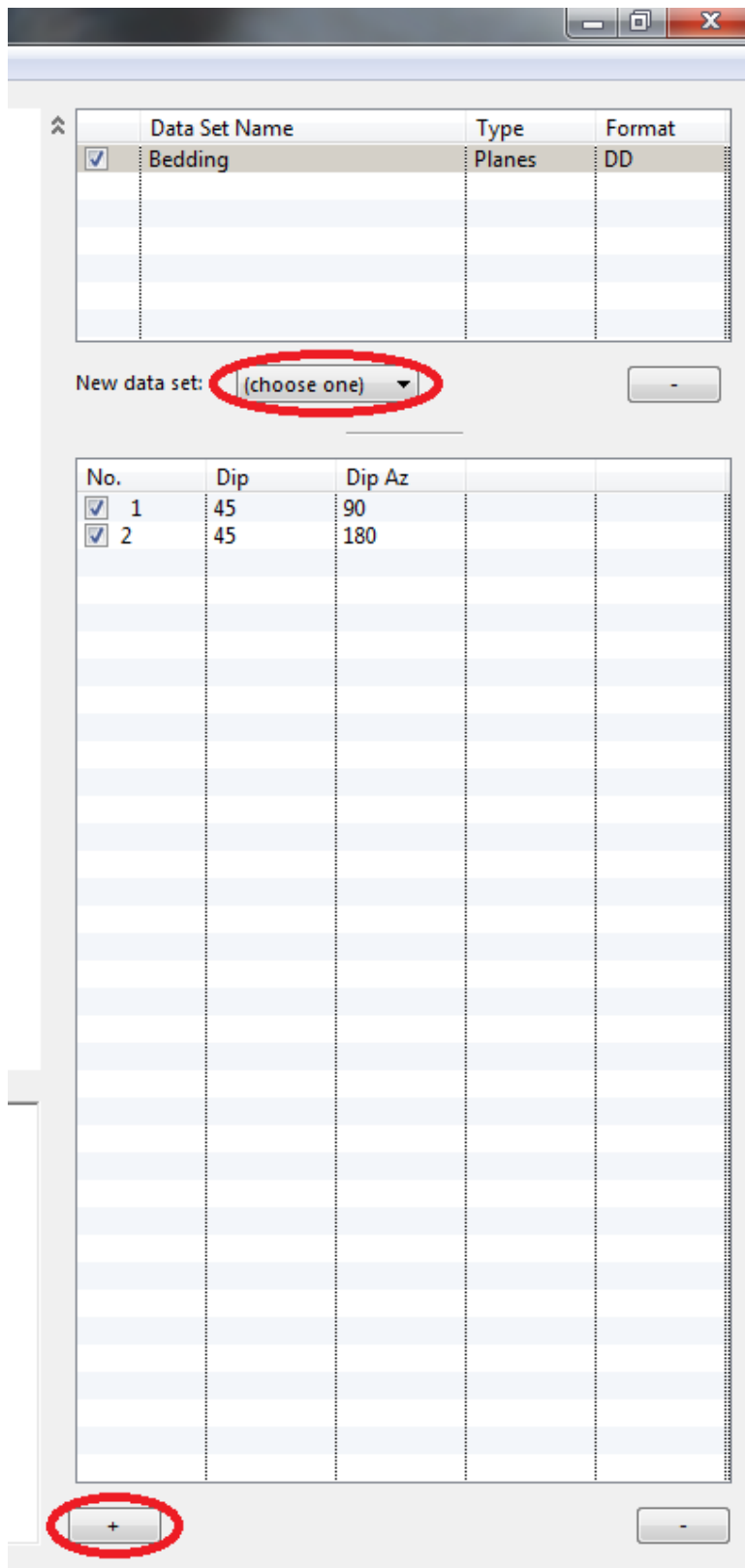
Open Stereonet 8 and select 'New blank window'

- 1) Under 'Window' tab select 'Preferences'

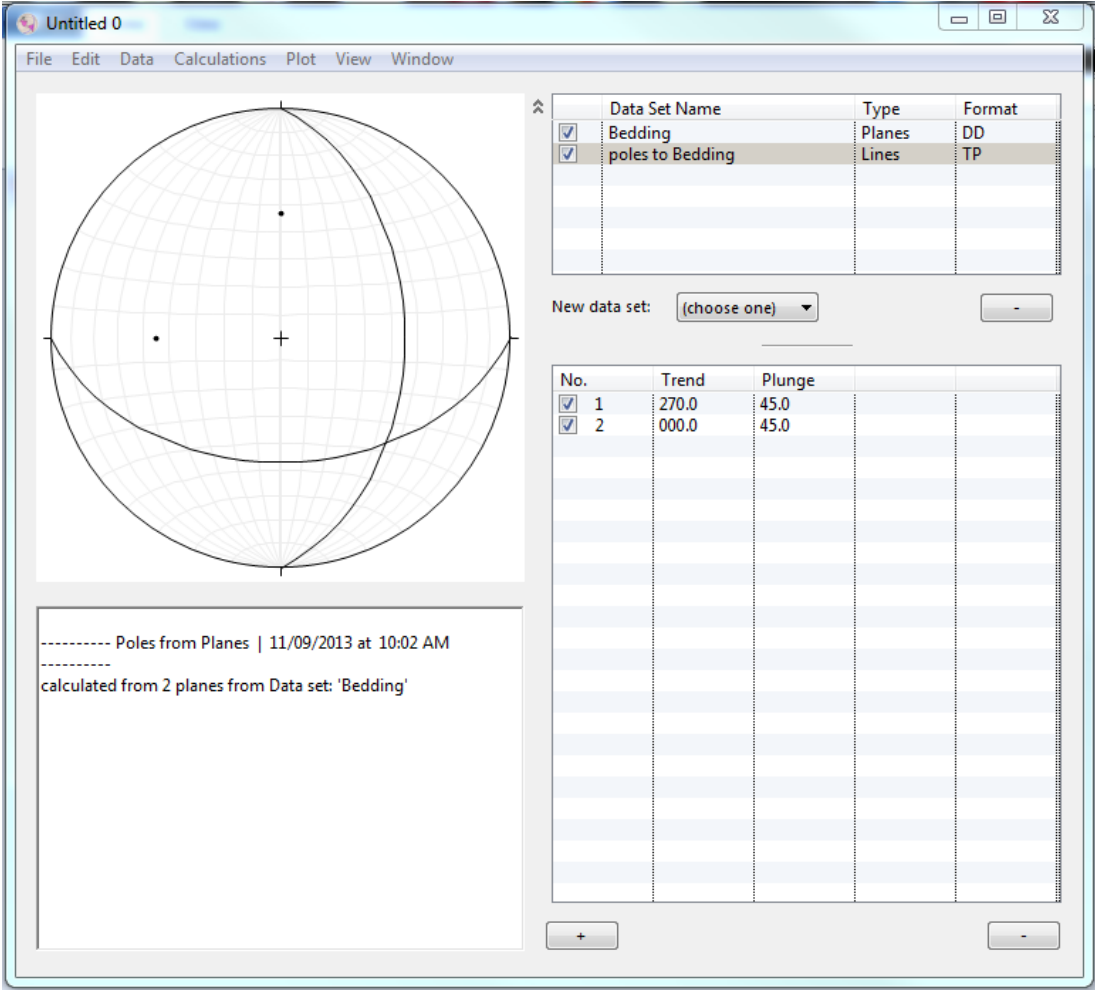


- Set 'Lines' to TP – Trend, Plunge
- Set 'Planes' to DD – Dip, Dip Azimuth
- Select 'Okay'

2) In the 'choose one' menu select 'planes' to create new data set. To add planes, click '+' then enter dip and dip azimuth values



3) To calculate poles to plan, in the 'calculations' drop down menu, select 'poles'



JRS Method - JRS Data Entry

1. Enter data into JRS Office Access 2000 file.

a) Under 'Field – Ref' tab, assign Field/s.

	Field	Field Name	Click to Add
+		4 Vic Otway	
+		8 Facemaps	
*		(New)	

b) Under 'Wellinfo' tab, enter field site names (or well) into new rows and assign a number corresponding to the field the well/site belongs to (from previous step)

	UWI	Well Name	Field
+	1	Castle Cove Eumeralla	4
+	2	Castle Cove Eocene	4
+	3	Crayfish Bay	4
+	4	Marengo	4
+	5	Skene's Creek	4
+	6	Smythe's Creek	4
+	7	Cape Patton	4
+	8	Cumberland River	4
+	9	Moonlight Head	4
+	10	Cape Otway	4
+	11	Lorne	4
+	12	Wongarra	4
+	13	Cape Otway Map 1	8
+	14	Cape Otway Map 2	8
+	15	Moonlight Head Map 1	8
+	16	Moonlight Head Map 2	8
+	17	Marengo Map 1	8
+	18	Marengo Map 2	8
+	19	Satellite Test Marengo	0
+	20	Satellite Test Skenes Cree	0
+	21	Castle Cove Map Proximal	8
+	22	Castle Cove Map Distal	8
+	23	CCP Update	8
+	24	CCD Update	8
*		(New)	0

c) Under the 'Frac Colour' tab, assign fracture types to a corresponding 'FracID' number. Then choose frac colour, marker type, line width to each fracture.

FracID	Frac Type	Frac Colour	Marker Type	Stipple	LineWidth	Factor	Alpha	AzLines	DisplayName
96	Field Fracture	clBlack	2	<input type="checkbox"/>	3	0	0.5	<input type="checkbox"/>	Field Interpreted Fracture
97	Strike Only	clBlack	2	<input type="checkbox"/>	3	0	0.5	<input type="checkbox"/>	Field Interpreted Fracture Strike Only
101	Calcite	clBlack	2	<input type="checkbox"/>	2	0	0.5	<input type="checkbox"/>	
102	Siderite	clBlack	2	<input type="checkbox"/>	2	0	0.5	<input type="checkbox"/>	
103	Quartz	clBlack	2	<input type="checkbox"/>	2	0	0.5	<input type="checkbox"/>	
104	Open Field Fracture	clBlack	1	<input checked="" type="checkbox"/>	3	0	0.5	<input type="checkbox"/>	Field Interpreted Fracture
105	Closed Field Fracture	clBlack	2	<input checked="" type="checkbox"/>	3	0	0.5	<input type="checkbox"/>	Field Interpreted Fracture
*	(New)			<input type="checkbox"/>	0	0	0	<input type="checkbox"/>	

d) Under the 'Fractures – Int' tab, begin to add data. UWI is the assigned UWI from step 1b, FracID is the assigned value from step 1c, Depth the depth at which the fracture was recorded, and Dip and DipDirn the dip and dip direction of the fracture.

UFracID	UWI	FracID	Depth (m)								Dip	DipDirn
12275	20	97	1								90	314
12276	20	97	1								90	314
12277	20	97	1								90	315
12278	20	97	1								90	315
12279	20	97	1								90	324
12280	20	97	1								90	341
12281	20	97	1								90	342
12282	20	97	1								90	346
12283	20	97	1								90	347
*	(New)	0	0									

JRS Roses

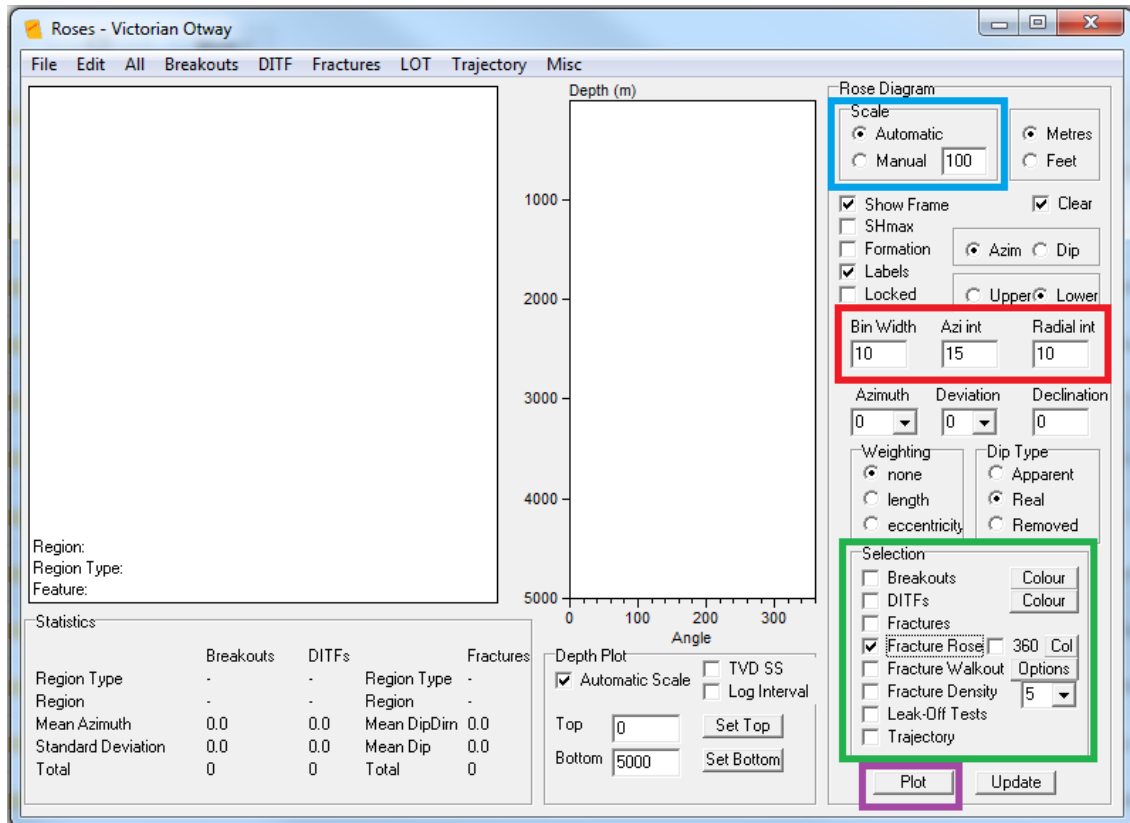
1. Open 'Roses' and select appropriate field.
2. Under 'Fracture' menu select 'Query'

The screenshot shows a 'Query Fractures' dialog box with the following settings:

- Wells:** Radio button 'Wells' is selected. The dropdown menu shows 'Well'.
- Fractures:** Check box 'All' is selected. Buttons for 'Fractures' and 'Not Fractures' are present.
- Depth:** Radio button 'All' is selected. Other options are 'Depth' (with 'top' and 'bottom' input fields) and 'Formation' (with a dropdown menu).
- Buttons:** 'Create SQL' (yellow box), 'Execute SQL' (blue box), and 'Cancel' are at the bottom.

Choose desired well in 'Well' drop down menu (highlighted red). Select desired fractures to be displayed on rose diagram under menu 'Fractures' (highlighted purple). First select 'Create SQL' (outlined yellow), then select 'Execute SQL' (highlighted blue).

3.



First assign desired scale, either 'Automatic' or 'Manual' (outlined blue). Then assign desired 'Bin Width,' azimuth interval 'Azi int' and radial interval 'Radial int' (outlined red). Select 'Fracture Rose' in selection tab (outlined green) and then select 'Plot' to plot rose diagram.

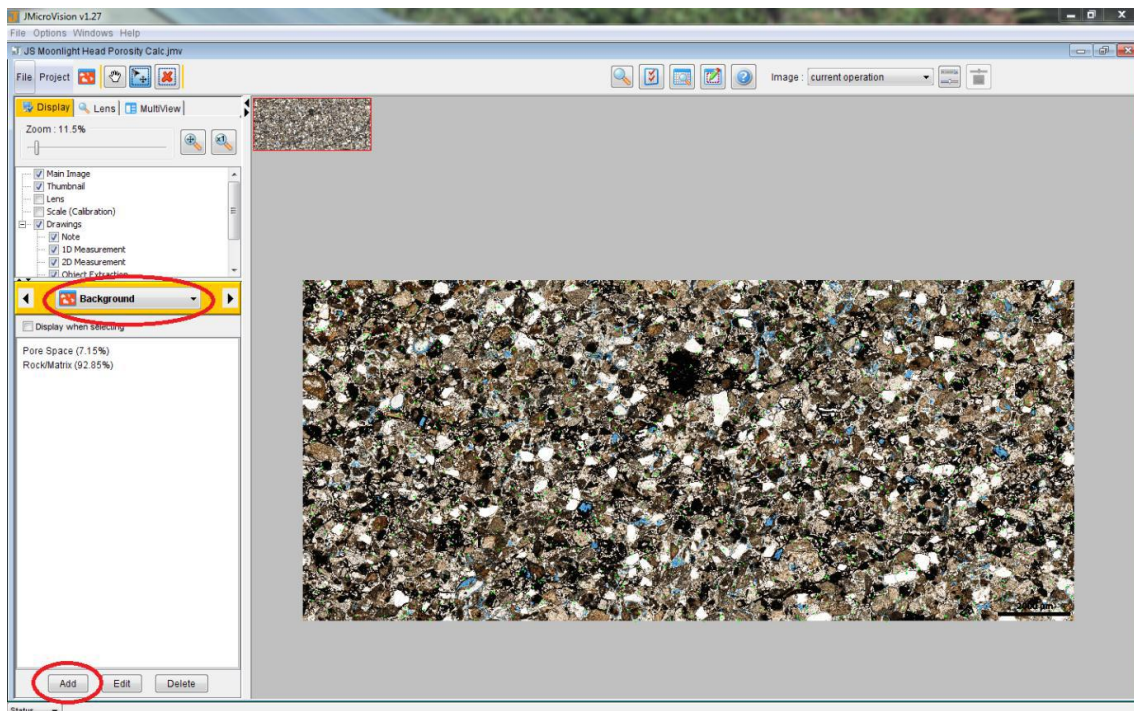
APPENDIX B: POROSITY

Porosity:

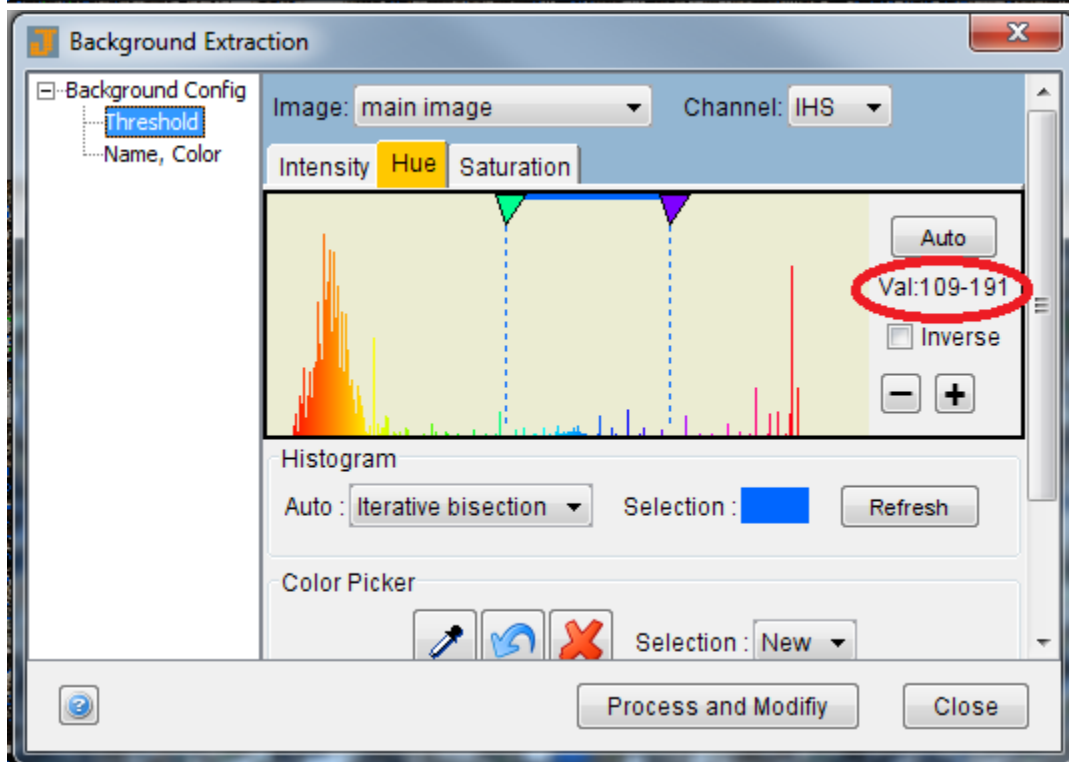
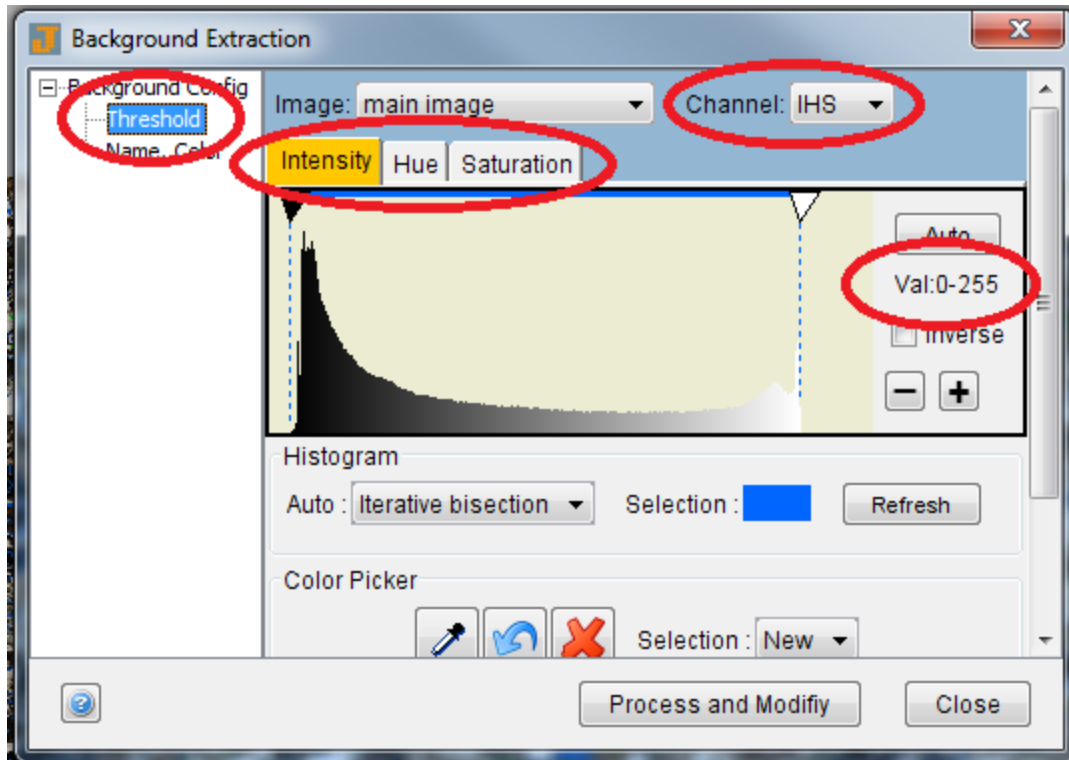
Using JMicroVision© V1.27, the image analysis technique was used to determine the porosity of 2 thin sections from the Otway Basin. The technique used is outline below.

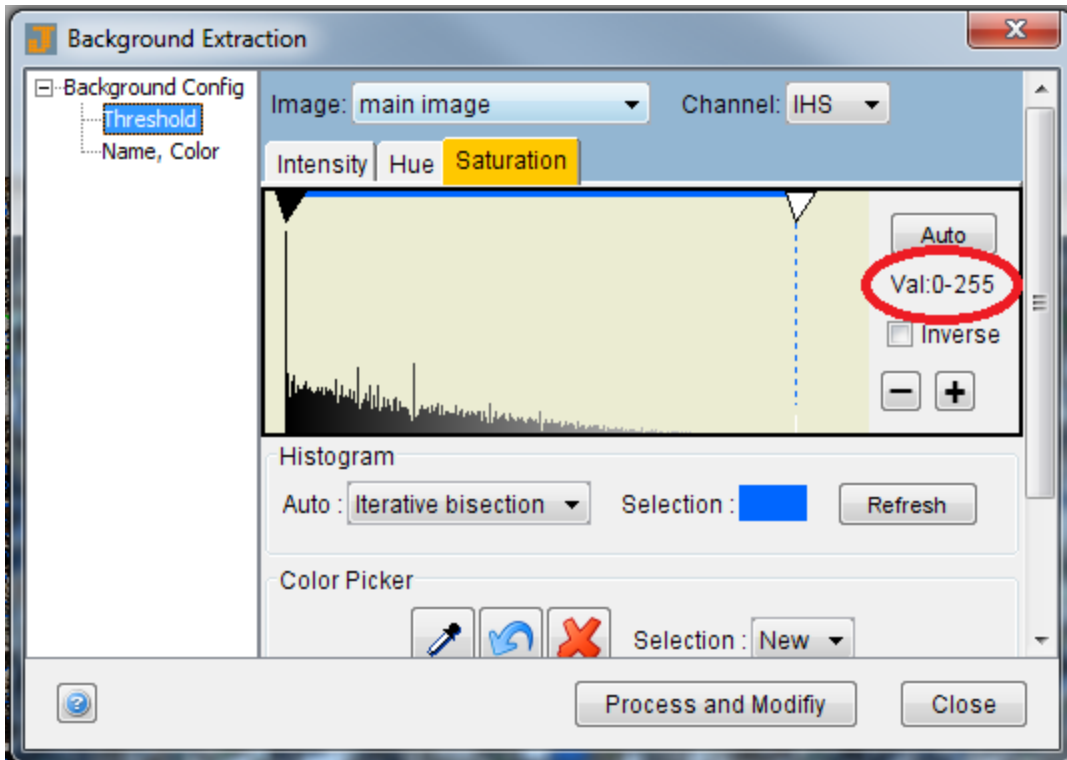
Image Analysis –

- 1) Load image into JMicroVision (Ctrl+I)
- 2) Select “Background” then “Add” to assign classes.

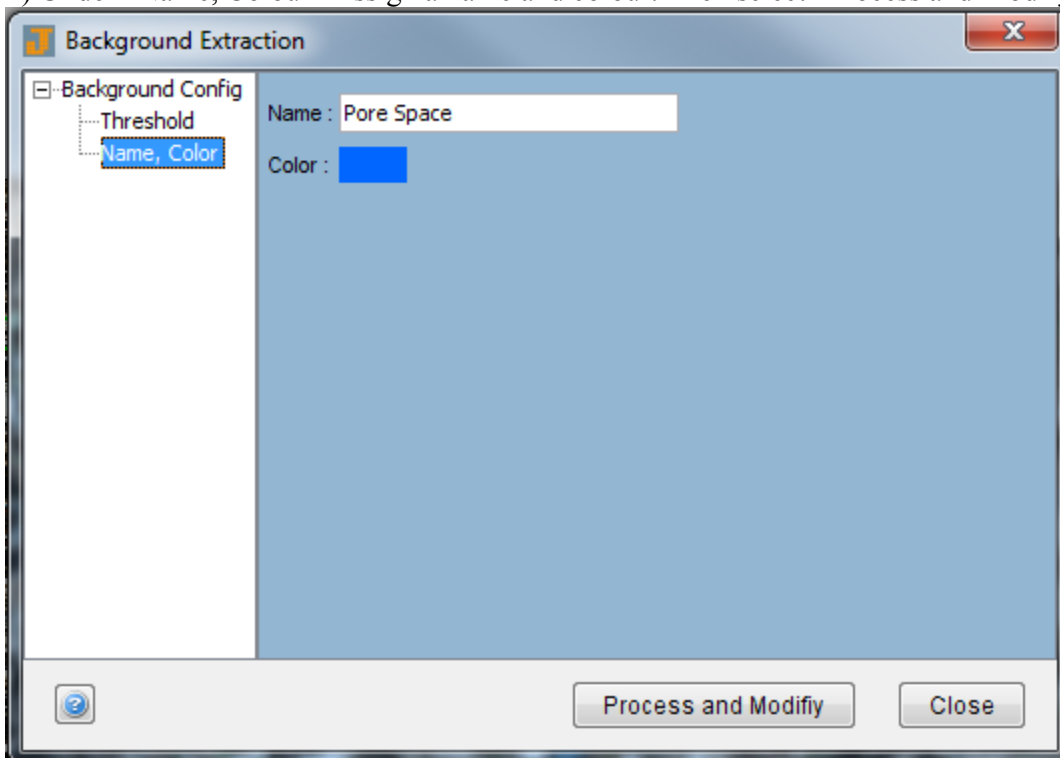


- 3) Under “Threshold” menu, choose “channel” as “HIS.” Set desired Intensity, Hue and Saturation.

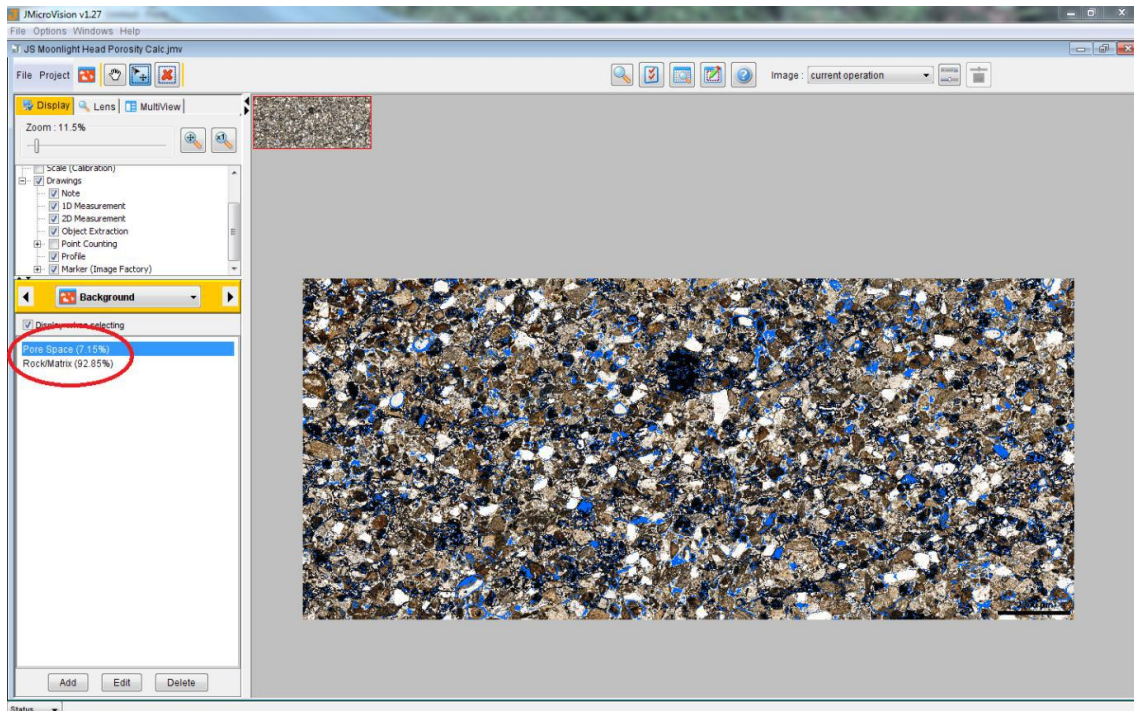




4) Under “Name, Colour” Assign a name and colour. Then select “Process and Modify”.



5) Repeat for all desired classes.



Absolute porosity (Core Samples)

- 1) Weight the core sample
- 2) Decompress the sample for 4 to 6 hours
- 3) Saturate the sample and let stand for 30 min
- 4) Re-weigh the sample and add the difference into percentage calculation with respect to the core sample volume.

APPENDIX C: EXTENDED FIELD MAPPING

FIELD MAPPING

This study employed two methods of deformation band measurements to attain data. Where vertical or near vertical faces were encountered at the field site, annotated face maps were drawn of the vertical face. Using grids of one metre squares, deformation bands and other important features of the face were drawn and measured. These grids ranged from 2.5 m to 6 m in height, and from 32m to 35 m in length. A tape measure was laid the length of the face and a one metre ruler placed vertically at the base of the face, with a bearing taken of the face map in the direction of the metre ruler. The GPS location of the start of the section and the end of the section was also recorded, including the accuracy of the GPS itself. A minimum of 3 metres of accuracy on all GPS readings was taken, where possible. A full list of face map locations, GPS readings, lengths, height and orientations is given in Face Map Table 1, Figure Location Map.

Where wave cut platforms were accessible in front of face maps, a series of grid maps were made. Using grids of one metre squares, in five metre squared areas, deformation bands and other important features were drawn and measured. A tape measure was placed at the base of the face map where the grid map corresponded and a measurement was taken of the length to the beginning of the wave cut platform from the face map. The GPS of the location of the grid map was also recorded, including the accuracy of the GPS itself. A full list of grid map locations, correlating face maps, length along face maps and distance from face maps is given in Grid Map Table 1, Figure Location Map. Location Map. A) bathometric and digital elevation image of Australia; B) close up of the St Vincent Basin and Adelaide Fold Belt, with red lines indicating faults (1, Willunga Fault, 2, Clarendon Fault and 3, Eden Fault) and a yellow star indicting the location of Sellicks Beach, and; C) satellite image of all locations where data were collected in the field area at Sellicks Beach.

Face map Table 1. Face map locations with GPS coordinates, length and orientation.

Face map no.	GPS Start		GPS End		Length of Face map	Height of Face map	Orientation of Face map
	Latitude	Longitude	Latitude	Longitude			
Face map 1	-35 ° 20 ' 6.58440 "	138 ° 26 ' 48.21727 "	-35 ° 20 ' 7.48906 "	138 ° 26 ' 48.03039 "	32 m	2.5 m	East 109°

Face map 2	-35 ° 20 ' 10.75013 "	138 ° 26 ' 47.25453 "	-35 ° 20 ' 11.84936 "	138 ° 26 ' 47.06153 "	35 m	3 m	East 092°
Face map 3	-35 ° 20 ' 16.44734 "	138 ° 26 ' 45.05550 "	-35 ° 20 ' 19.21507 "	138 ° 26 ' 42.43381 "	33.5 m	6 m	East 113°
Face map 4	-35 ° 20 ' 20.36995 "	138 ° 26 ' 41.80340 "	-35 ° 20 ' 21.16643 "	138 ° 26 ' 41.10507 "	33 m	4 m	East 124°
Face Map 5	-35 ° 20 ' 24.11721 "	138 ° 26 ' 39.46761 "	-35 ° 20 ' 25.24468 "	-35 ° 20 ' 25.24468 "	35 m	3 m	East 124°

Grid map Table 2. Wave-cut platform grid map locations, correlating face map number with length along face map, distance from face map and GPS coordinates.

Grid map no.	Correlating Face map no.	GPS		Length along Face map	Distance form Face map
		Latitude	Longitude		
Grid map 1	4	-35 ° 20 ' 20.62330 "	138 ° 26 ' 39.97372 "	28 m – 33 m	31 m
Grid map 2	4	-35 ° 20 ' 20.23834 "	138 ° 26 ' 40.18386 "	15 m – 20 m	32 m
Grid map 3	5	-35 ° 20 ' 25.05490 "	138 ° 26 ' 37.77474 "	30 m – 35 m	31 m

STRUCTURAL DATA COLLECTION

Face maps - As deformation bands were encountered along the face map, they were drawn (using a lead pencil), numbered, and the distance along and height on the face map was recorded. The dip and dip direction of the deformation band was measured. If this was not possible, the strike orientation of the deformation band was measured. The aperture width of the deformation band, aperture style (see aperture style for details), cement fills and cross cutting relationship with other deformation bands were noted. As suitable bedding surfaces were encountered along the face map, they were drawn, numbered and the distance along and height on the face map was recorded. The dip and dip direction of the bedding was measured.

When recording data a number was placed on the sketch next to its corresponding deformation band or bedding surface and the data collected on a spreadsheet (see data collection spreadsheet of details). A list of structural measurements is recorded in the Structural Measurements Table.

Grid maps – As deformation bands were encountered, they were drawn (using a lead pencil) and numbered on the grid map. The strike of the deformation band was measured. The number was recorded on the sketch next to its corresponding deformation band and the data recorded in a notebook.

Structural Measurements Table. List of structural measurements collected and the type of measurement.

Measurement	Type of measurement
Deformation Band Plane	Dip and Dip Direction
Deformation Band Strike (Used for grid measurements and when a plane was unattainable on a Face map).	Strike
Bedding	Dip and Dip Direction

DATA COLLECTION SPREADSHEET

Figure. Data collection spreadsheet. Spreadsheet used to collect data acquired from face maps.

DATA COLLECTION SPREADSHEET VARIABLES

Distance: Length was measured by running a 50 m tape measure along the base of the face map, marking the corresponding deformation band in metres along the tape measure. Height was measured using a one metre ruler, placing it at the base of the face map, with data recorded in metres. Deformation bands measured above one metre in height were measured by marking the metre height on the wall face, then placing the ruler at this mark (at zero metres on the ruler) and adding the values together.

Deformation band (Dip and Dip): the dip and dip direction of a deformation band was measured with a compass clinometer and notebook. The notebook was placed in

Reading number	Distance (m) (length – height)	Deformation band (Dip and Dip)	Aperture width	Aperture (sharp, gradual, diffuse)	Deformation band Fill	Bedding (Dip and Dip)	Sedimentary structures
1	3.55 – 1.55	12/125	2 – 3 mm	Sharp	Micrite	N/A	N/A

reference to the deformation bands dip (as an extension of the deformation band). The compass clinometer was placed on the notebook and the measurement collected.

Aperture width: the aperture width was taken using a ruler (with millimetre values), by placing the ruler horizontally across the deformation band, recording from where the band visibly began with respect to the host rock. Values recorded were entered as millimetre intervals (2 – 3 mm) and whole numbers (2 mm).

Aperture (sharp, gradual, diffuse): see aperture style for a list of details.

Deformation band Fill: three fills were recorded in this study, reorientated bioclasts, black lithic inclusions and micrite fill.

Reorientated bioclasts: weathered bioclasts, reorientated in alignment with respect to each other (Figure 2, Reorientated bioclasts).



Figure 2) reorientated bioclasts within a sharp deformation band.

Black lithic inclusions: addition of black lithics within reorientated bioclast deformation bands, predominantly observed within weathered sections along bands (Figure 3, Black lithic inclusions).

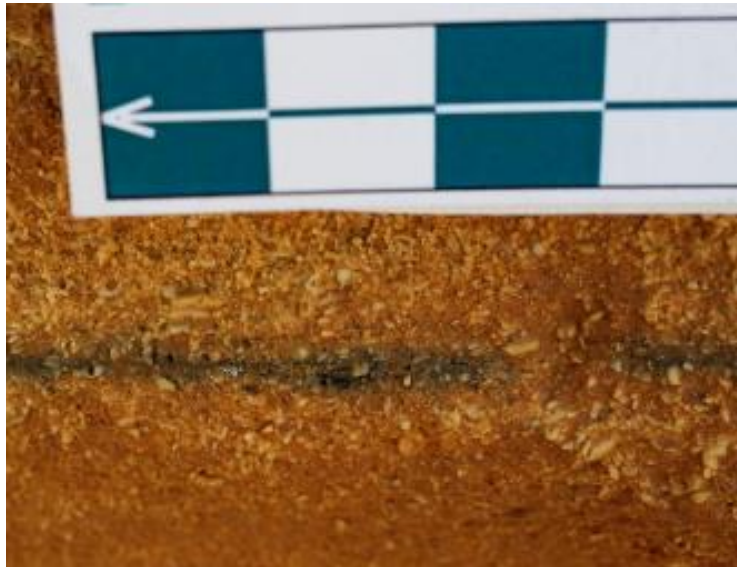


Figure 3) black lithics within a Sharp deformation band.

Micrite fill: predominantly hosted by sharp deformation bands, occasionally containing small amounts of bioclasts (Figure 4, Micrite fill).



Figure 4) sharp micrite fill deformation band, hosting small amounts of individual bioclast grains.

Bedding (Dip and Dip): the dip and dip direction of bedding was measured with a compass clinometer and notebook. The notebook was placed in reference to the beds dip angle as an extension refernec to the bedding plane. The compass clinometer was placed on the notebook and the measurement collected.

Sedimentary structures: this section was for any extra information that was relevant to the deformation band or bedding been collected e.g. lateral cross-bedding associated with this bedding reading indicates the younging direction to be upwards.

APERTURE STYLE

A list of defining features which separate deformation band aperture types, categorized as: 1) Sharp; 2) Gradual, and; 3) Diffuse (Figures 5 to 8).

- 1) Sharp: distinct change in lithology between deformation band and host rock, commonly comprising of different coloration between the two .e.g. deformation band containing micrite infill and a bioclastic grainstone host rock (Figure 5).

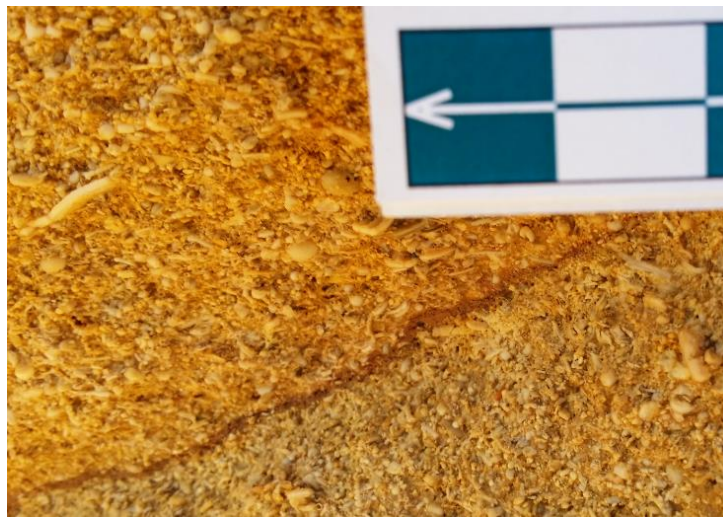


Figure 5) sharp deformation band with micrite fill, hosting small amounts of individual bioclast grains.

OR

A distinct visual change from randomly orientated bioclasts too aligned bioclasts within the deformation band aperture zone (Figure 6).



Figure 6) sharp deformation and of reorientated bioclasts, with its borders indicated by red outline.

- 2) Gradual: Obvious zones within the deformation band's aperture, an inner zone containing distinct alignment of bioclasts and outer zones where bioclasts display sub-alignment, although, still distinct from host rock (Figure 7).

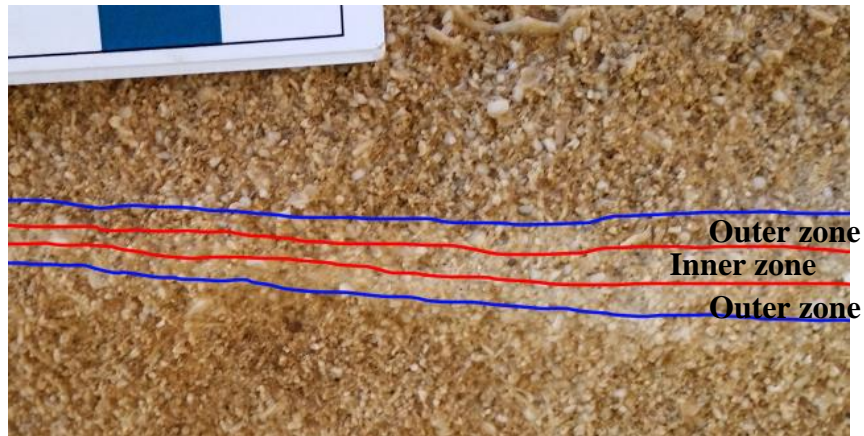


Figure 7) gradual deformation band, the inner zone of aligned bioclasts within the red lines, and outer zones of sub-aligned bioclasts defined the blue lines.

- 3) Diffuse: aligned to sub-aligned bioclasts within the inner zone of the deformation band, and poorly distinguishable outer zones of irregularly aligned bioclasts, which grade into the host rock (Figure 8).

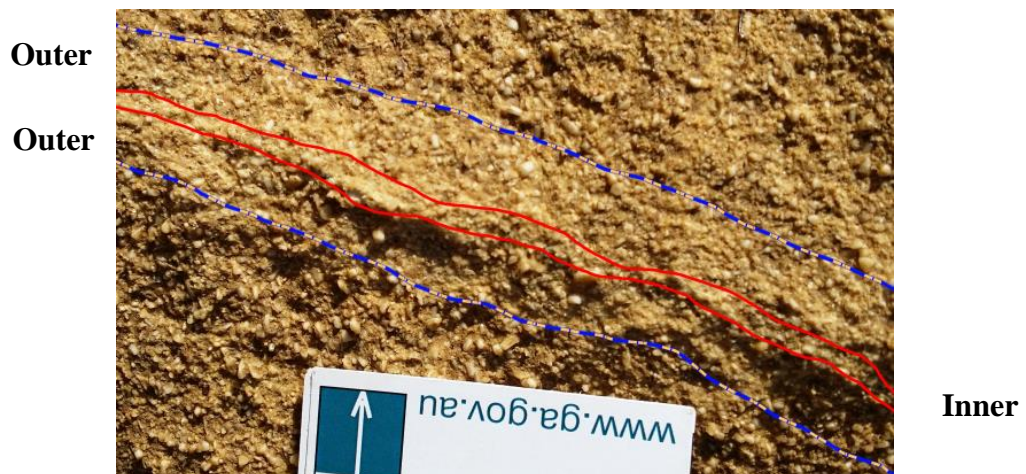
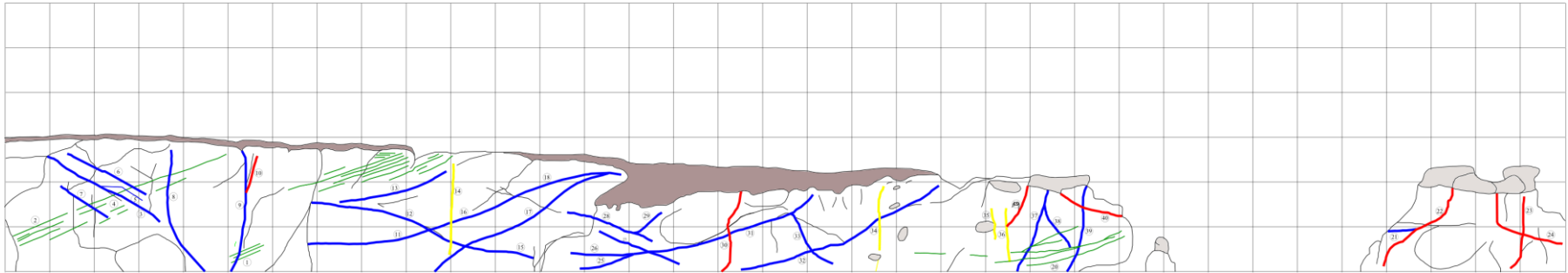


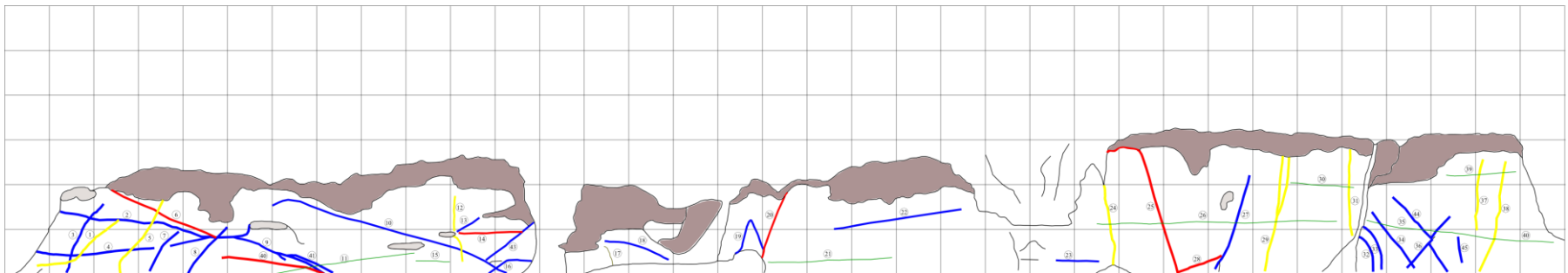
Figure 8) diffuse deformation band, red lines indicating the inner zone, and the dashed blue lines indicating the inferred limits of the outer zones of the deformation band.

APPENDIX D: FACE MAPS 1 TO 5

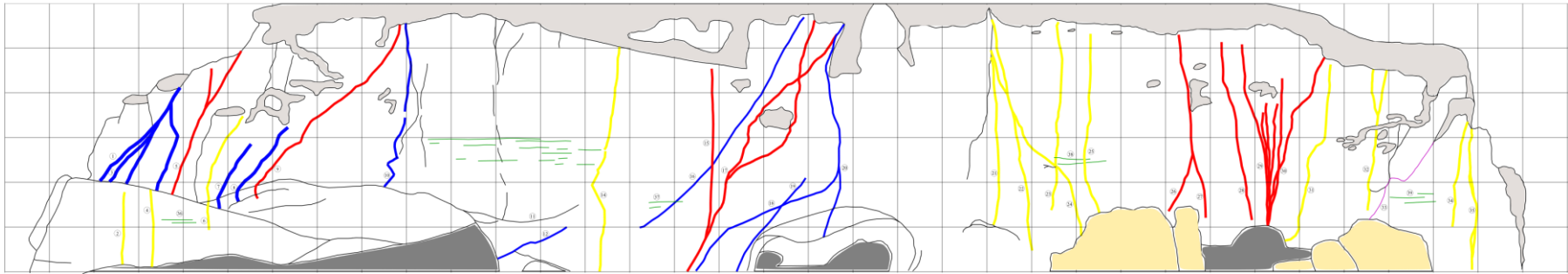
Face map 1



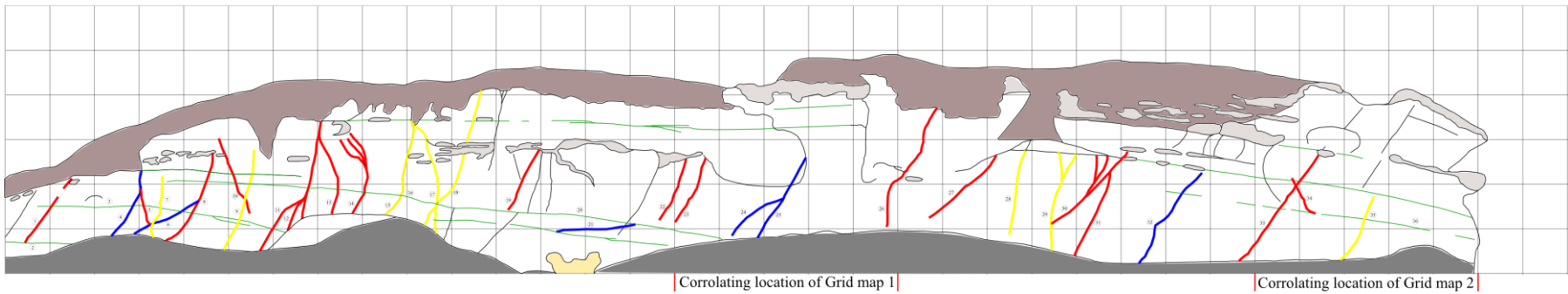
Face map 2



Face map 3



Face map 4



Face map 5

